

PB83 - 203554



U.S. Department
of Transportation

Federal Railroad
Administration

Analysis of Thermal Buckling Tests on U.S. Railroads

Office of Research and
Development
Washington, DC 20590

Andrew Kish
Gopal Samavedam
David Jeong

DOT/FRA/ORD-82/45

November 1982

This document is available to the
U.S. public through the National
Technical Information Service,
Springfield, Virginia 22161.

REPRODUCED BY
U.S. DEPARTMENT OF COMMERCE
NATIONAL TECHNICAL
INFORMATION SERVICE
SPRINGFIELD, VA 22161

NOTICE

This document is disseminated under the sponsorship of the Department of Transportation in the interest of information exchange. The United States Government assumes no liability for its contents or use thereof.

NOTICE

The United States Government does not endorse products or manufacturers. Trade or manufacturers' names appear herein solely because they are considered essential to the object of this report.

1. Report No. FRA/ORD-82/45		2. Government Accession No.		3. Recipient's Catalog No. PB8 3 203554	
4. Title and Subtitle Analysis of Thermal Buckling Tests on U.S. Railroads				5. Report Date November 1982	
				6. Performing Organization Code DTS-743	
7. Author(s) A. Kish, G. Samavedam*, and D. Jeong				8. Performing Organization Report No. DOT-TSC-FRA-82-6	
9. Performing Organization Name and Address U.S. Department of Transportation Research and Special Programs Administration Transportation Systems Center Cambridge, MA 02142				10. Work Unit No. (TRAIS)	
				11. Contract or Grant No. RR-219	
12. Sponsoring Agency Name and Address U.S. Department of Transportation Federal Railroad Administration Office of Research and Development Washington, D.C. 20590				13. Type of Report and Period Covered Interim June 1981 - December 1981	
				14. Sponsoring Agency Code DOT/FRA/RRD-32	
15. Supplementary Notes *Foster-Miller Associates, Inc. 350 Second Avenue Waltham, MA 02154					
16. Abstract Thermal buckling of railroad tracks in the lateral plane is an important problem in the design and maintenance of continuous welded rails (CWR). The severity of the problem is manifested through the increasing number of derailments which are attributable to track buckling, indicating a need for developing better control on the allowable, safe temperature increase for CWR track. The work reported here is a part of a major investigation conducted by the Transportation Systems Center (TSC) for the Federal Railroad Administration (FRA), on the analytical predictions of critical buckling loads and temperatures, supported by experimental verification on an operating mainline railroad in the U.S. The experimental work consisted of two major tests at The Plains, VA, conducted as part of a cooperative research program with the Southern Railway System. One test was on tangent track and the other on curved. Both test zones were fully instrumented for compressive forces, temperatures, lateral and longitudinal displacements. Analyses of the two test results, theoretical predictions and conclusions of practical significance are presented. Supplemental test results conducted by the Southern Railway on non-instrumented track and results of earlier rail heating tests are also included.					
17. Key Words track buckling, track lateral stability, buckling tests, buckling analysis, continuous welded rail (CWR).			18. Distribution Statement Document is available to the U.S. public through the National Technical Information Service, Springfield, VA 22161		
19. Security Classif. (of this report) Unclassified		20. Security Classif. (of this page) Unclassified		21. No. of Pages 102	22. Price

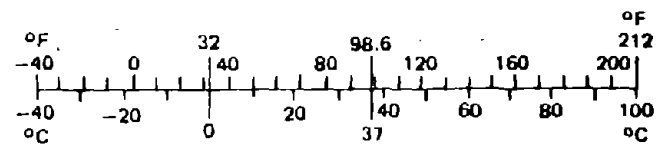
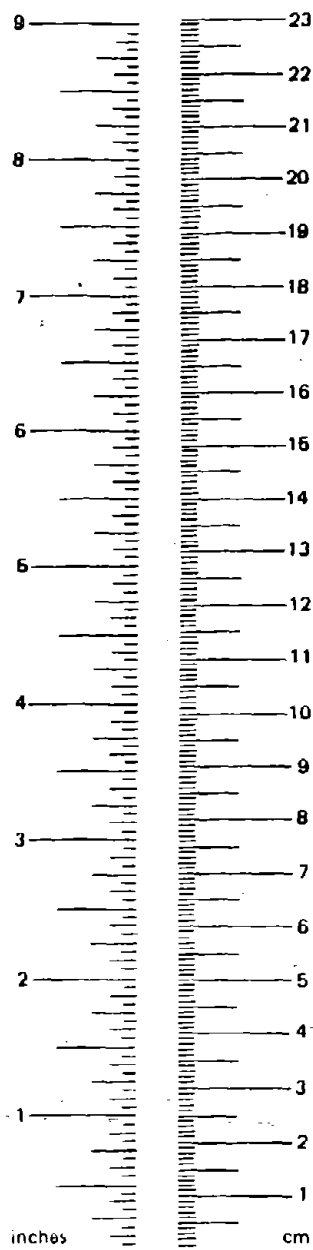
METRIC CONVERSION FACTORS

Approximate Conversions to Metric Measures

Symbol	When You Know	Multiply by	To Find	Symbol
LENGTH				
in	inches	2.5	centimeters	cm
ft	feet	30	centimeters	cm
yd	yards	0.9	meters	m
mi	miles	1.6	kilometers	km
AREA				
in ²	square inches	6.5	square centimeters	cm ²
ft ²	square feet	0.09	square meters	m ²
yd ²	square yards	0.8	square meters	m ²
mi ²	square miles	2.6	square kilometers	km ²
	acres	0.4	hectares	ha
MASS (weight)				
oz	ounces	28	grams	g
lb	pounds	0.45	kilograms	kg
	short tons (2000 lb)	0.9	tonnes	t
VOLUME				
tsp	teaspoons	5	milliliters	ml
Tbsp	tablespoons	16	milliliters	ml
fl oz	fluid ounces	30	milliliters	ml
c	cups	0.24	liters	l
pt	pints	0.47	liters	l
qt	quarts	0.95	liters	l
gal	gallons	3.8	liters	l
ft ³	cubic feet	0.03	cubic meters	m ³
yd ³	cubic yards	0.76	cubic meters	m ³
TEMPERATURE (exact)				
°F	Fahrenheit temperature	5/9 (after subtracting 32)	Celsius temperature	°C

Approximate Conversions from Metric Measures

Symbol	When You Know	Multiply by	To Find	Symbol
LENGTH				
mm	millimeters	0.04	inches	in
cm	centimeters	0.4	inches	in
m	meters	3.3	feet	ft
m	meters	1.1	yards	yd
km	kilometers	0.6	miles	mi
AREA				
cm ²	square centimeters	0.16	square inches	in ²
m ²	square meters	1.2	square yards	yd ²
km ²	square kilometers	0.4	square miles	mi ²
ha	hectares (10,000 m ²)	2.5	acres	
MASS (weight)				
g	grams	0.035	ounces	oz
kg	kilograms	2.2	pounds	lb
t	tonnes (1000 kg)	1.1	short tons	
VOLUME				
ml	milliliters	0.03	fluid ounces	fl oz
l	liters	2.1	pints	pt
l	liters	1.06	quarts	qt
l	liters	0.26	gallons	gal
m ³	cubic meters	36	cubic feet	ft ³
m ³	cubic meters	1.3	cubic yards	yd ³
TEMPERATURE (exact)				
°C	Celsius temperature	9/5 (then add 32)	Fahrenheit temperature	°F



² 1 in. = 2.54 cm (exactly). For other exact conversions and more detail tables see NBS Misc. Publ. 286, Units of Weight and Measures, Price \$2.25 SD Catalog No. C13 1D 286.

PREFACE

Under the Federal Railroad Administration's (FRA) Improved Track Structures Program, the Transportation Systems Center (TSC) is conducting research to develop the engineering basis for more effective track safety guidelines and specifications. The intent of these specifications is to ensure safe train operations while allowing the industry maximum flexibility for cost-effective track engineering and maintenance practices.

One of the major safety issues currently under investigation under this program deals with track buckling. The work reported here is part of this investigation dealing with the analytical prediction of critical buckling loads and temperatures, supported by experimental verification on an operating mainline railroad.

The authors would like to thank Messrs. C.H. Perrine and H.D. Reed of the Transportation Systems Center, Messrs. R. Krick and W.B. O'Sullivan of the Federal Railroad Administration for their helpful comments and review of the report, and Mr. W.S. Lovelace of the Southern Railway System for providing invaluable assistance in conducting the tests.

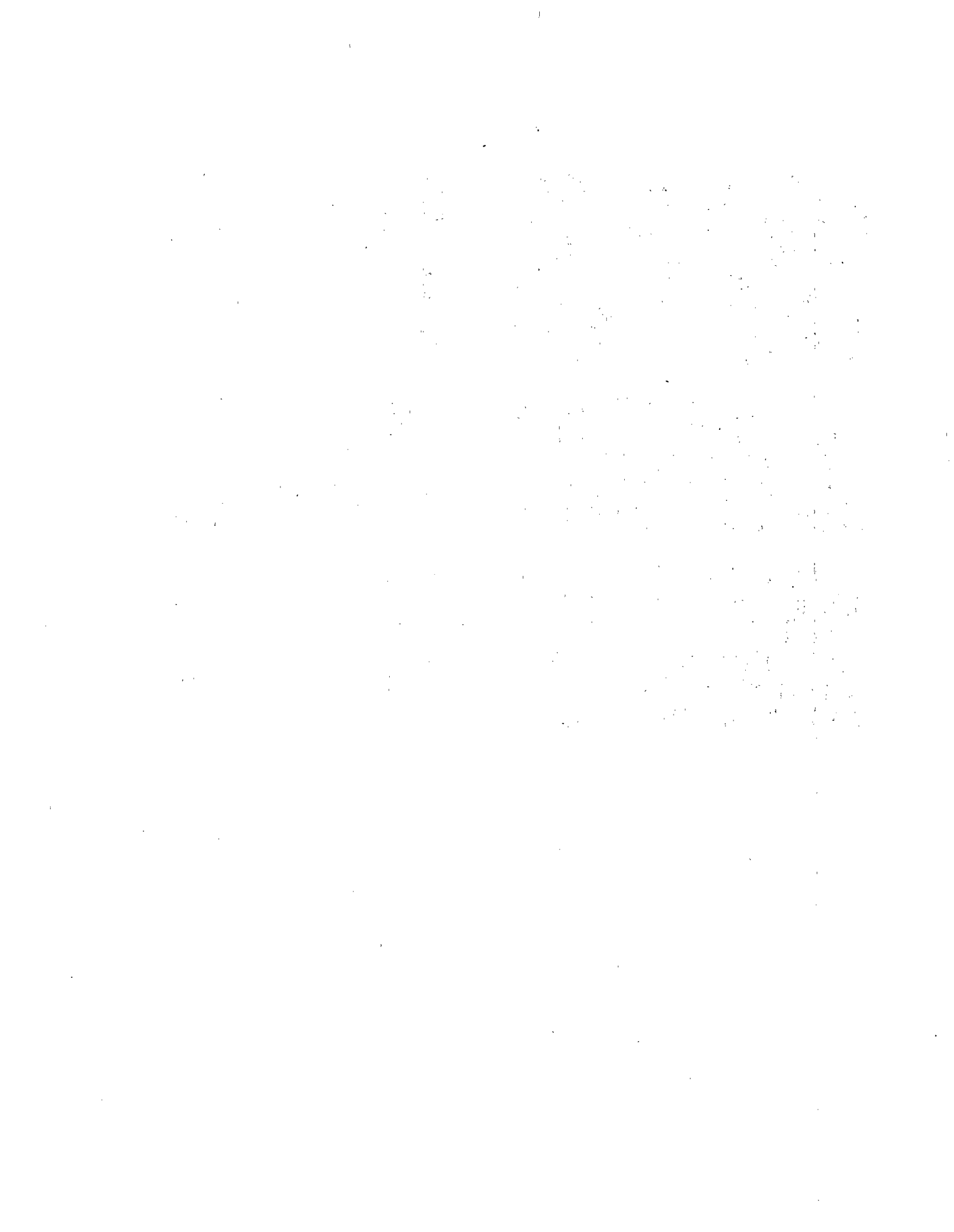


TABLE OF CONTENTS

<u>Section</u>	<u>Page</u>
1. INTRODUCTION	1
2. BUCKLING RESEARCH REVIEW	3
2.1 Review of Past Work	3
2.2 Scope of the Present Work	4
3. TEST CONDUCT	7
3.1 Tangent Track	7
3.2 Curved Track	12
4. TRACK PARAMETERS	20
4.1 Stress-free Temperature	20
4.2 Initial Misalignment	20
4.3 Lateral Resistance	23
4.4 Longitudinal Resistance	29
4.5 End Stiffness	32
4.6 Summary	32
5. GENERAL THEORY	37
5.1 Equations for Breathing Zone	37
5.2 Equations for Buckling Zone (Tangent Track)	40
5.3 Equations for Buckling Zone (Curved Track)	45
5.4 Computational Scheme	47
6. TANGENT TRACK ANALYSES	48
6.1 Temperature-Deflection Response	48
6.2 Rail Force-Deflection Response	48
6.3 Buckled Wave Shape	51
6.4 Rail Force Variation	51
6.5 Longitudinal Displacement Variation	55
6.6 Summary	57
7. CURVED TRACK ANALYSES	59
7.1 Temperature-Deflection Response	59
7.2 Rail Force-Deflection Response	59
7.3 Buckled Wave Shape	59
7.4 Rail Force Variation	63
7.5 Tangential Displacement Variation	63
7.6 Summary	66

Preceding page blank

TABLE OF CONTENTS (CONTINUED)

<u>Section</u>	<u>Page</u>
8. CONCLUSIONS	70
9. RECOMMENDATIONS	71
REFERENCES	73
APPENDIX A - ADDITIONAL TESTS AT THE PLAINS, VA	A-1
APPENDIX B - PILOT TESTS AT CHATTANOOGA, TN	B-1
APPENDIX C - PHOTOGRAPHS FROM THE PLAINS, VA, TRACK BUCKLING TESTS	C-1

LIST OF FIGURES

<u>Figure</u>		<u>Page</u>
1	Tangent Track Instrumentation	9
2	Loading Apparatus for Lateral Resistance	11
2-1	Displacement Measurement for Lateral Resistance Test	11
2-2	Lateral Resistance Function	11
3	Tangent Track Heating Rate	14
4	Curved Track Instrumentation	16
5	Curved Track Heating Rate	19
6	Stress-Free Temperature (Tangent Track)	21
7	Stress-Free Temperature (Curved Track)	22
8	Misalignment Setting (Tangent Track)	24
9	Misalignment Setting (Curved Track)	25
10	Longitudinal Force Distribution (Tangent Track)	31
11	Longitudinal Force Distribution (Curved Track)	33
12	End Stiffness Computation (Tangent Track)	34
13	End Stiffness Computation (Curved Track)	35
14	Illustrating the Effects of Finite Length, l , and End Stiffness, k	38
15	Buckling Mode Shapes	41
16	Temperature-Deflection Response (Tangent Track)	49
17	Rail Force vs. Maximum Deflection (Tangent Track)	50
18	Buckled Wave Shape III (Tangent Track)	52
19	Rail Force Buildup (Tangent Track)	53
20	Rail Force Variation Before and After Buckling (Tangent Track)	54
21	Longitudinal Displacement (Tangent Track)	56
22	Temperature-Deflection Response (Curved Track)	60

LIST OF FIGURES (CONTINUED)

<u>Figure</u>		<u>Page</u>
23	Rail Force vs. Maximum Deflection (Curved Track)	61
24	Buckled Wave Shape I (Curved Track)	62
25	Rail Force Buildup (Curved Track)	64
26	Rail Force Variation Before and After Buckling (Curved Track)	65
27	Longitudinal Displacement (Curved Track)	67
28	Buckling Response in the Lateral Plane	69

LIST OF TABLES

<u>Table</u>		<u>Page</u>
1	Rail Properties (Tangent and Curved) and Track Parameters (Measured or Derived)	8
2	Typical Output from Datalogger (Tangent Track)	13
3	Buckled Mode Shapes for Tangent and Curved Tests	15
4	Typical Output from Datalogger (Curved Track)	18
5	Summary of Comparison Between Theory and Experimental Values (Tangent Track)	58
6	Summary of Comparison Between Theory and Experimental Values (Curved Track)	68
7	Summary of SR Buckling Tests (Curved Track)	A-2

LIST OF PHOTOGRAPHS

		<u>Page</u>
1	Curved Test Site	C-2
2	Tangent Test Site	C-2
3	Initial Misalignment Setting and Lateral Resistance Measurement	C-3
4	Locomotive/Rail Heating	C-3
5	Strain Gauge Setup	C-4
6	Apparatus for Setting Initial Imperfection and Measurement of Lateral Response	C-4
7	Buckled Wave Shape III (Tangent Track)	C-5
8	Ballast Disturbance from Buckled Shape (Tangent)	C-5
9	Buckled Wave Shape I (Curved Test)	C-6
10	Buckled Wave Shape from Curved Test	C-6

LIST OF SYMBOLS AND ABBREVIATIONS

x	longitudinal distance from center of track
E	Young's Modulus for rail steel
A	Rail cross-sectional area
I	Rail area moment of inertia about the vertical axis
ΔT	Rail temperature (above the stress-free temperature)
ΔT_S	Safe temperature (above the stress-free temperature)
ΔT_B	Buckling temperature (above the stress-free temperature)
\bar{P}	Rail compressive force in the buckled zone
P	Compressive force in the rails
P_L	Applied lateral force in track resistance test
w	lateral deflection
U	axial displacement in the buckled zone
u	axial displacement in the adjoining zone
w'	primes denote derivatives with respect to x
\dot{w}	dots denote derivatives with respect to θ
α	coefficient of thermal expansion
F_0	constant lateral resistance
f_0	constant longitudinal resistance
$2l$	test track length
$2L$	buckling length
$2L_1$	length of middle half wave in Shape III
$2L_0$	length of misalignment
δ_0	misalignment amplitude
k	end stiffness
β	PL^2/EI
t	ratio L_1/L
R	radius of curvature
A_m	Fourier coefficients for w , deflection
a_m, b_m	Fourier coefficients as defined in text
l_1	distance between zero longitudinal displacement and center of track

SUMMARY

The increased utilization of continuous welded rail (CWR) in U.S. tracks has resulted in an increasing number of accidents attributable to derailments induced by thermal buckling of railroad tracks. In an effort to improve the safety of CWR, experimental and analytic investigations were conducted by the Transportation Systems Center (TSC) supporting the safety mission of the Federal Railroad Administration (FRA). This report describes these investigations, and presents the results applicable for improved safety, design and maintenance practices.

The experimental work primarily consisted of two full-scale mainline thermal buckling tests on the Harrisonburg Line of the Southern Railway. These tests, one on tangent, the other on a curved segment, included instrumentation to measure compressive forces, temperatures, lateral and longitudinal displacements, and track lateral resistance.

The results of the tests were utilized in the development and validation of analytic models for the prediction of the lateral buckling response for tangent and curved tracks in the absence of vehicle induced loads. The analytic models developed are capable of predicting buckling temperatures, the "safe" temperature increase, critical forces, and pre- and post-buckling displacements, in the presence of imperfections and finite (short) test section influences.

The buckling analyses verification studies showed that the theoretical predictions are in good agreement with the test data resulting in an improved understanding of the track buckling mechanism. On the basis of the experiments and theoretical studies, the following major results and conclusions are presented:

1. Both tangent and curved track exhibited relatively high buckling temperatures (above neutral), in spite of initial imperfections.
2. The curved track exhibited a lower buckling temperature than the tangent, a less "explosive" type of buckling, and a smaller buckled wave shape and amplitude.
3. Measured values of lateral and longitudinal resistances were in the range of 54 to 83 lb/in and 69 to 87 lb/in, respectively, which can be taken as representative values for "good" track based on the SR test track conditions.
4. The importance of adequate test section length was manifested by the non-uniform axial force build-up and test section end displacements, resulting in the improvement of analytic predictions by including pre-buckled displacements and end-restraint parameters.
5. Established test concepts, techniques and methodologies for the conduct of full-scale buckling tests utilizing locomotives as a power source for rail heating.

1. INTRODUCTION

Thermal buckling of tracks in the lateral plane is an important problem in the design and maintenance of continuous welded rails. The severity of the problem can be seen from Ref. [1] where it is indicated that during the period 1976-1979, there were at least 100 derailments in each year attributable to track buckling. The reported number of derailments in 1980 was 174, which caused an estimated damage of \$14.2 million. More significantly, for every buckling accident that caused a derailment, it has been estimated that there were at least 10 buckling incidents noted and corrected by timely track maintenance [2].

Current methods used by the track design and maintenance engineers to minimize the risk of track buckling are empirical. Adequate designs need to account for the proper buckling temperature within a factor of safety. Given the maximum rail temperature, T_M , attained in the yearly cycle, the design may be based on the criterion $\Delta T_B = f_s (T_M - T_n)$ where ΔT_B is the buckling temperature increase, T_n is the neutral temperature and f_s is the factor of safety. Clearly, the higher T_n is, the larger the safety factor will be. However, in winter when the rail temperature drops to its minimum T_m , there will be a large tensile stress proportional to $(T_n - T_m)$, which, in conjunction with wheel load stresses, may lead to rail fatigue fracture. Therefore, it is important to optimize the rail neutral temperature, taking into account the regional variations of the maximum and the minimum temperatures. The only guideline available in the U.S. in this regard seems to be the AREA recommended practice [3], which specifies a laying temperature range around the expected mean temperature.

The problem is further complicated because of possible deviations of the neutral temperature from the rail installation temperature. Rail de-stressing from time to time may be required. Track maintenance-of-way engineers need to know simple inspection pro-

cedures to assess the neutral temperature and economic methods to increase the buckling strength of service tracks, if required.

From the foregoing, it is seen that a number of problems of practical significance need to be resolved in the area of thermal response of continuous welded rails. The current empirical knowledge of track buckling is clearly not satisfactory, as evidenced from the continued interest and need by the railroad engineers in the U.S. and abroad, for a better understanding of the buckling phenomenon and dependable safety specifications. Therefore, in 1978, the Federal Railroad Administration (FRA) initiated a major research program on this subject, with the ultimate aim of development of recommendations on the safety standards to minimize the number of derailments due to track buckling. The Transportation Systems Center supports the FRA in the conduct of the program by providing technical direction of and involvement in the research activities.

The work reported here is a part of a major investigation conducted by TSC on the analytical predictions of critical buckling loads and temperatures, supported by experimental verification on operating mainline railroads in the U.S. The experimental work consisted of two major tests at The Plains, VA, one on a tangent track and the other on a curved track. The purposes of these tests were to compare the buckling mechanism for tangent and curved track and to validate recently developed analytic models. Both test zones were fully instrumented for compressive forces, temperatures, and lateral and longitudinal displacements. Analyses of the two test results, theoretical predictions, and conclusions of practical significance are presented here.

A brief description of four additional tests performed without instrumentation at The Plains, VA, and the two pilot tests carried out earlier at Chattanooga, TN, is also presented.

2. BUCKLING RESEARCH REVIEW

2.1 REVIEW OF PAST WORK

A brief review of the past theoretical and experimental work will be presented here. On the theoretical side, numerous publications exist; the majority of the published work used incorrect or inadequate formulations and are not suitable for buckling analyses as discussed by Kerr [4]. Under certain simplifying assumptions, Kerr [5] presented a post-buckling analysis for tangent tracks without imperfections; his analysis was intended for the determination of the safe temperature increase and not the buckling temperatures.*

To study the effect of track imperfections, nonlinearities in track parameters, missing ties, and vehicle and other external loads, a versatile method has been developed by Samavedam [6], which yields both the safe and buckling temperature increases. Parametric studies and design data for CWR utilization in Great Britain have also been presented.

Samavedam in [6] has also presented a theory for the curved track with imperfections, which is the only curved track buckling theory available which predicts both the safe and the buckling temperature increases.

Buckling experiments were conducted by several railway organizations in the past. The majority of the tests were poorly designed and, in some cases, led to erroneous conclusions. In the tests by Ammann and Gruenewaldt [7], and by Nemcsek [8], the rail compressive force was induced by hydraulic jacks, which is not a suitable method to simulate the thermal buckling phenomenon. Birmann and Raab [9] of the German Federal Railways conducted rail heating/buckling experiments on a 150.9 ft. (46 m)

*Refer to Figure 28 for a definition of safe temperature increase and buckling temperature.

long track. As shown later, the test track was too short for the results to be representative of the infinite track. Bartlett [10] of the British Railways experienced a similar shortcoming by using a short track of about 118.1 ft. (36 m) long. Nemesdy [11] and later Nagy [12] of the Hungarian Railways carried out tests on a 629.8 ft. (192 m) long track. Although the results were meant for empirical use, they indicated for the first time the influence of track curvature and moving loads on track. Bromberg [13] of the USSR railways conducted tests on a 328 ft. (100 m) long track, and his results too were meant for an empirical use. In view of the complexity of the phenomenon of track buckling, empirical use of results is of questionable validity.

In 1979, Samavedam [14], then with the British Railways, conducted a set of buckling tests on a specially built track at Old Dalby, England. The track was 328 ft. (100 m) long, with end concrete blocks (sunk into the ground) to prevent end longitudinal movements. The rails were heated by direct current, obtained by rectifying alternating current from a three-phase 440 volt supply. The track was instrumented with strain gauges and displacement transducers. Buckling tests were conducted on a tangent concrete tie track, with the aim of validating Samavedam's straight track analyses [6]. In the tests, it was found that end movement of the concrete blocks occurred, which resulted in a varying prebuckling compressive force in the rails. The theory was later modified to incorporate the end movement due to the finite stiffness at the ends. Reasonable agreement between the theory and the experiment was found [14]. Additional tests were carried out in 1980, which included buckling under an external lateral load and a moving vehicle.

2.2 SCOPE OF THE PRESENT WORK

In contrast to the European test programs involving specially built test tracks, the U.S. buckling test program centered directly on mainline service tracks. This was motivated by the fact that the practical use of a theory can be appreciated only

when tested in realistic situations. The test results obtained were also of direct use to railroad engineers.

Mainline buckling tests are typically not undertaken because of the difficult technical and logistical problems posed by such a large-scale test program. Some problems and the solutions used in the tests reported herein are briefly discussed here.

- (1) Heating Equipment: It is clear that the heating equipment could not be permanently housed at one location. A mobile apparatus was needed. The use of diesel electric locomotives to supply current to the rails as used in the Hungarian tests [12] was found to be most suitable source of rail heating. This concept was successfully demonstrated for the first time in the U.S. at Chattanooga in conjunction with two pilot buckling tests conducted cooperatively with the Southern Railway (Appendix 2).
- (2) Track Resistance Characterization: Track parameters (lateral and longitudinal resistances) have to be characterized and measured in a convenient manner with as little disruption to traffic as possible. Existing methods of parameter measurement were found to be inadequate and new approaches described in later chapters were developed. A mobile rig for measuring lateral resistance was specially designed and fabricated.
- (3) Instrumentation: The track occupancy time is generally extremely limited for minimum disruption of traffic. Rapid deployment of instruments such as strain gages, lateral and longitudinal transducers, and temperature transducers was imperative. The rail heating and buckling experiment had to be completed in less than two hours' time. For fast recording of data, a Datalogger was used.

- (4) Test Section Length: The problem of minimum test section length had to be re-examined, previous analytic considerations being inadequate because of the finite stiffness at the junctions between the heated and the unheated rails. Fundamental studies were carried out to analyze the behavior of finite tracks with finite stiffness [16]. This resulted in the choice of 656 ft. (200 m) as the test section length.

3. TEST CONDUCT

The two tests mentioned in Section 1 (one on a tangent track and the other on a 5° curved track) were performed during the period of 21-23 June 1981, on the Harrisonburg Line of the Southern Railway in the town of The Plains, VA. The tests were designed in accordance with the requirement set forth in [17] and conducted as planned in the experiment design [18]. Participating in the tests were personnel from the Federal Railroad Administration (FRA), Transportation Systems Center (TSC), Foster Miller Associates, Inc. (FMA), the Southern Railway, and Portec, Inc. The data collected during the tests were entered in the Buckling Test Data File, available at TSC.

3.1 TANGENT TRACK

The track had 132 lb continuous welded relay rails on wood ties at 20-inch spacing, on a good quality granite ballast with 12"-14" shoulder. Alternate ties were box anchored. The test section was 656 ft. (200 m) long. A central portion of the test section was tamped to simulate a recently weakened condition. The rail and the track properties are listed in Table 1. Although the annual tonnage is approximately 1.2 million gross tons (MGT), the track was maintained to mainline quality standards.

Instrumentation: The primary instrumentation for the buckling test consisted of eleven strain gauges (SG_1 - SG_{11}), four temperature transducers (T_1 - T_4), three longitudinal displacement transducers (U_1 - U_3), and one lateral displacement transducer. The deployment of the instruments is shown in Figure 1.

The strain gauges were compensated for bending and thermal strains and directly yielded the force in the rail. The strain gauges and the bridge circuit were tested in the laboratory prior to the application in the field tests.

TABLE 1 - RAIL AND TRACK PARAMETERS

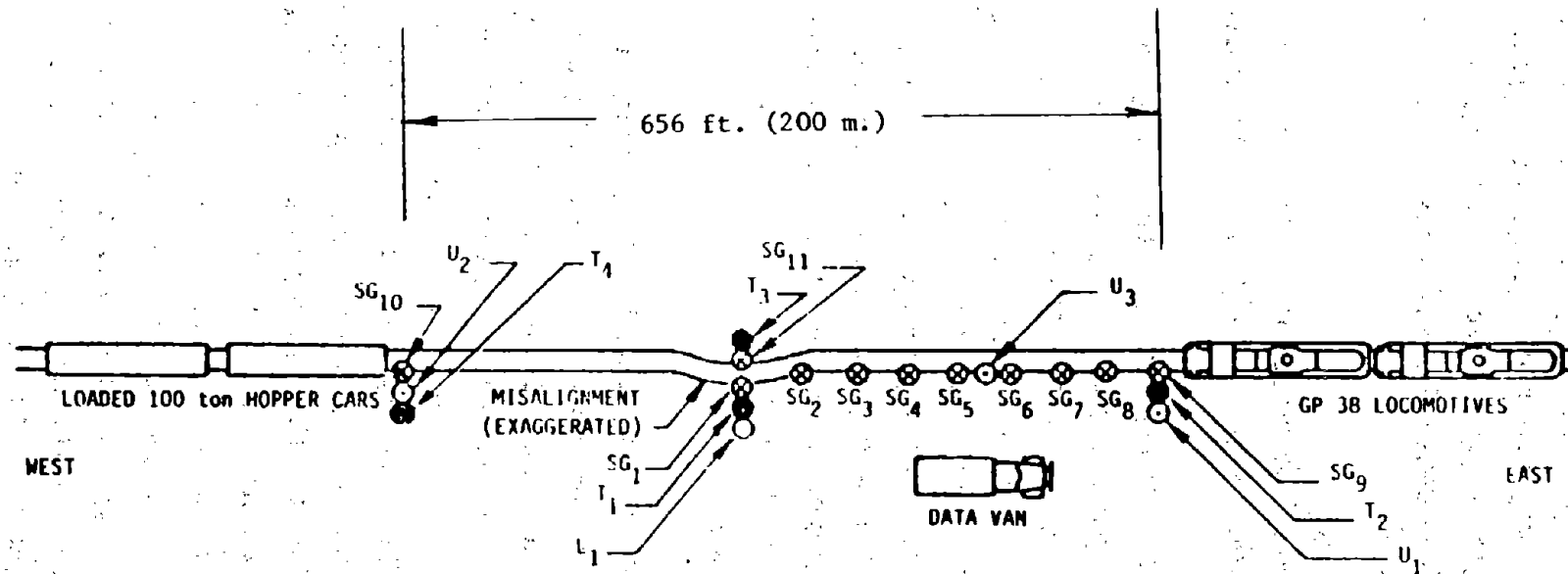
RAIL PROPERTIES

WEIGHT:	132 LB./YD.
YOUNG'S MODULUS, E:	30×10^6 PSI
AREA MOMENT OF INERTIA, $2I_{ZZ}$:	2×14.2 IN. ⁴
CROSS SECTIONAL AREA, $2A$	2×12.95 IN. ²
COEFFICIENT OF THERMAL EXPANSION, α :	$6.39 \times 10^{-6}/^{\circ}F$

TRACK PARAMETERS

(MEASURED OR DERIVED)

	TANGENT	CURVED
BALLAST TYPE	GRANITE	GRANITE
RAIL ANCHOR	EVERY OTHER TIE	EVERY OTHER TIE
GRADE	0.6%	0.3%
TIE SPACING	20 INCHES	20 INCHES
TIE MATERIAL	WOOD	WOOD
SHOULDER WIDTH	10-14 INCHES	12-16 INCHES
TEST LENGTH, $2L$	656 FT. (200 M)	656 FT. (200 M)
NEUTRAL TEMPERATURE	71.3°F (21.8°C)	72.3°F (22.4°C)
MISALIGN. AMPLITUDE, δ_0	1.6 IN. (41 MM)	1.5 IN. (38 MM)
MISALIGN. LENGTH, $2L_0$	36 FT. (11 M)	36 FT. (11 M)
LATERAL RESISTANCE, F_0	54.3 LB/IN (972 KG/M)	83.3 LB/IN (1490 KG/M)
LONG. RESISTANCE, f_0	69.3 LB/IN (1240 KG/M)	87.2 LB/IN (1560 KG/M)
END STIFFNESS, k	1.12×10^9 LB/IN (2×10^7 KG/M)	1.12×10^9 LB/IN (2×10^7 KG/M)
RADIUS OF CURVATURE, R	∞	1148 FT. (350 M)



- 6
- LEGEND
- ⊗ STRAIN GAUGE (SG), 11 [DEPLOYED AT 41 ft. (12.5 m.) INTERVALS]
 - TEMPERATURE DETECTOR (T), 4
 - LATERAL DISPLACEMENT TRANSDUCER (L), 1
 - ⊙ LONGITUDINAL DISPLACEMENT TRANSDUCER (U), 3

FIG. 1 - TANGENT TRACK INSTRUMENTATION

The 19 transducers were monitored and read at frequent intervals during the test by means of a Datalogger. In addition, three X-Y plotters were used to obtain the real-time graphical output between SG_1 vs. L_1 (rail force-lateral deflection response), T_1 vs. L_1 (temperature-lateral deflection response) and SG_9 vs. U_1 (end stiffness).

A magnetic tape recorder was also used to record the output from the transducers and served as a standby for the datalogger.

Test Procedure: In the early morning of the buckling test day, the rail anchors were removed, the rails were cut at the ends of the test section and de-stressed for the purpose of providing a known, uniform, stress-free temperature in the rails and also to give a zero reference level for the output of the strain gauges. The joints were closed subsequently, using four insulated joints, and the track was re-anchored. During the re-anchoring process, rail temperature and the strain gauge readings were recorded. These data are needed to determine the correct stress-free temperature.

Prior to the installation of the insulated joints, a lateral misalignment was set at the center using the lateral pull rig designed for an earlier test at Readville, MA. The rig applied a lateral force at the center. At various lateral force levels, P_L , the lateral displacements at x_i ($i=0,1,2,3$) (Figure 2) were measured using string pot type displacement transducers. When a maximum imperfection amplitude of 2 in. (51 mm) was reached, the lateral load was removed. The track recovered a few millimeters and resulted in a final permanent set of 1.61 in. (41 mm) over a length of 36.1 ft. (11 m). This constituted the Shape I type misalignment (see Figure 15) for use in the buckling analysis. The final misalignment shape was measured relative to a string line. The load-deflection data collected in the misalignment setting were needed for computing the lateral resistance.

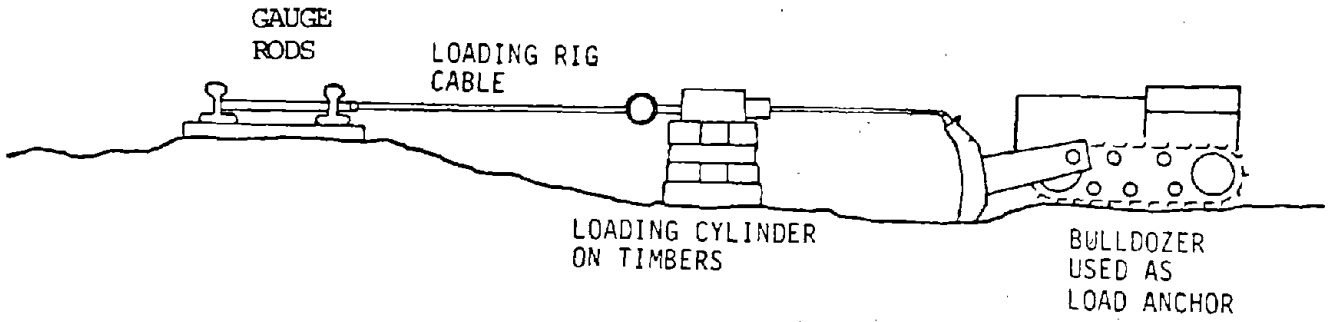


FIG. 2 - LOADING APPARATUS FOR LATERAL RESISTANCE TEST

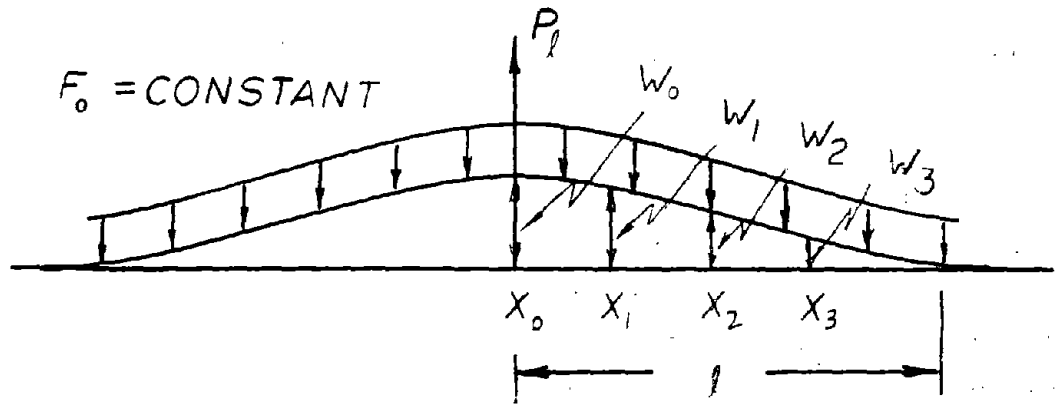


FIG. 2.1 - DISPLACEMENT MEASUREMENT FOR LATERAL RESISTANCE TEST

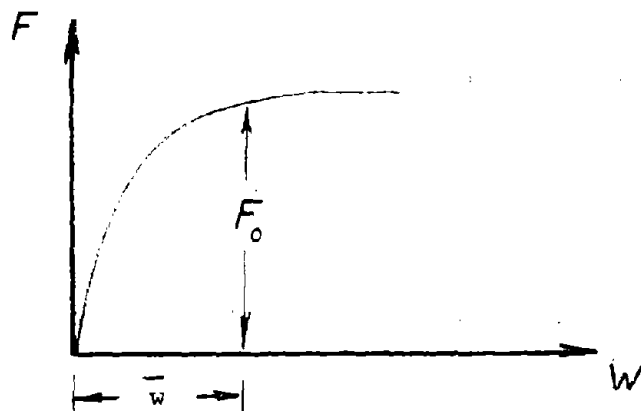


FIG. 2.2 - LATERAL RESISTANCE FUNCTION

After the foregoing operations, the electric resistance heating of the rails was started. The current was supplied by the two diesel electric locomotives especially converted to utilize their alternators as a heating source. The locomotives were stationed at one end of the test section, while two hopper cars were placed at the other end to provide symmetrical and restraint conditions.

Initially, a low current (<1000 amperes) was sent through the rails to check all the instruments for proper functioning, after which the current was increased and kept between 4000-6000 amperes. The current strength was again reduced prior to reaching the estimated buckling temperature and the datalogging frequency was increased until the track buckled. Typical outputs from the Datalogger are shown in Table 2 and the rate of heating in Figure 3.

After the track buckled, the current was shut off, and the buckled wave shape was measured. The resulting mode shape can be seen in Table 3. The heating was restarted and continued for another 15 minutes to obtain additional data on the post-buckling response of the track. The deformed rails incurred sufficient yielding as to require replacement.

3.2 CURVED TRACK

The track for this test was similar to the tangent track except for a curvature of 5°. The test length was 656 ft. (200 m). The procedure was similar to that described for the tangent track.

Instrumentation: The instrument deployment is shown in Figure 4. As in the tangent track, the instrumentation consisted of 11 strain gauges (SG_1 - SG_{11}), four temperature transducers (T_1 - T_4), three longitudinal displacement transducers (U_1 - U_3), and one lateral displacement transducer. In addition, four lateral displacement transducers (L_2 - L_5) were used to study the radial

TABLE 2 - TYPICAL OUTPUT FROM DATALOGGER
(TANGENT TRACK)

Reproduced from
best available copy.

019 *	11.3559	INS.	L 1	019 *	-8.72484	INS.
018 *	0.45584	INS.	U 3	018 *	0.57688	INS.
017 *	0.81715	INS.	U 2	017 *	0.75377	INS.
016 *	0.68146	INS.	U 1	016 *	0.58557	INS.
015	223.587	BEG-F	T 4	015	223.588	BEG-F
014	207.852	BEG-F	T 3	014	207.332	BEG-F
013	197.036	BEG-F	T 2	013	196.796	BEG-F
012	216.109	BEG-F	T 1	012	217.469	BEG-F
011	178.915	TONS	SG 11	011	67.8148	TONS
010	-97.2358	TONS	SG 10	010	-70.8433	TONS
009	-89.9591	TONS	SG 9	009	-56.8552	TONS
008	-100.818	TONS	SG 8	008	-57.5202	TONS
007	-108.931	TONS	SG 7	007	-53.7946	TONS
006	-123.313	TONS	SG 6	006	-51.5551	TONS
005	-130.648	TONS	SG 5	005	-48.5636	TONS
004	-147.478	TONS	SG 4	004	-41.1813	TONS
003	-149.194	TONS	SG 3	003	-37.8735	TONS
002	-149.525	TONS	SG 2	002	-33.3358	TONS
001	-153.631	TONS	SG 1	001	-53.3813	TONS
11:56:14 JUN 25, 1961				11:57:14 JUN 25, 1961		
TANGENT				TANGENT		

BEFORE BUCKLING

AFTER BUCKLING

* TO BE ADJUSTED FOR INITIAL VALUES

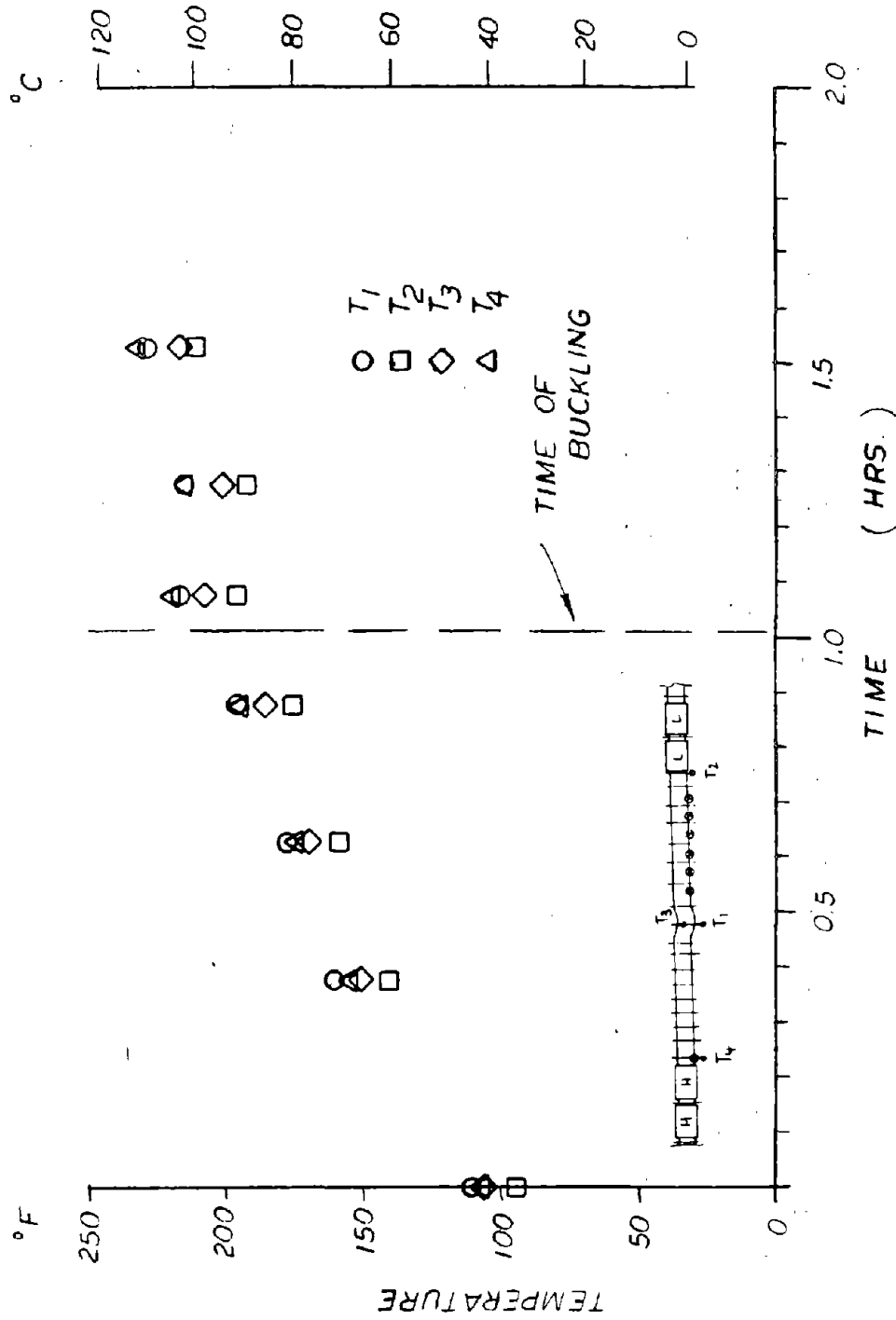
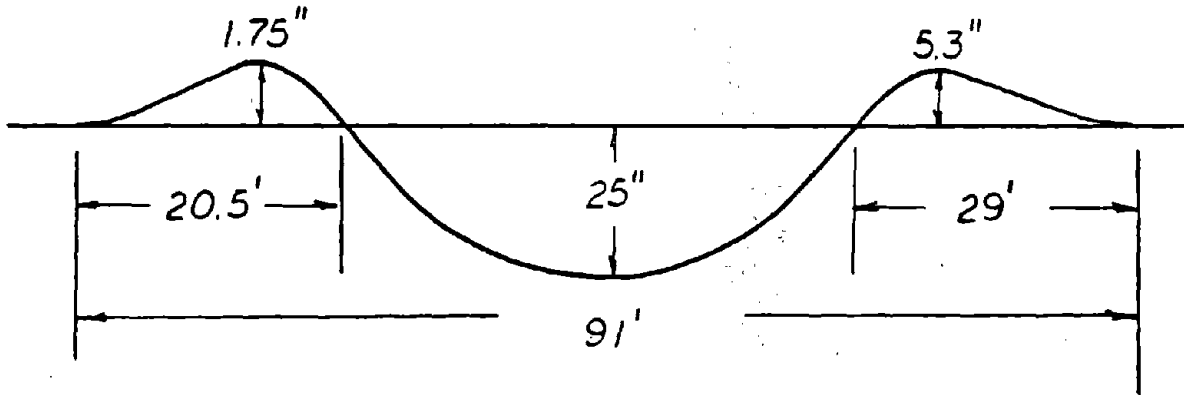


FIG. 3 - TANGENT TRACK HEATING RATE

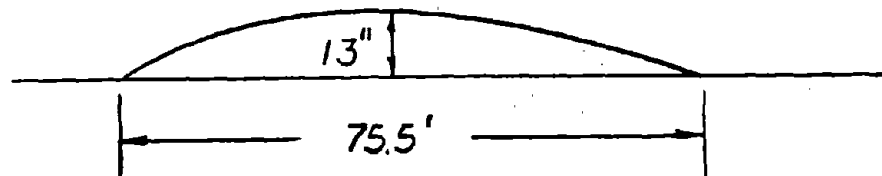
TABLE 3: BUCKLED MODE SHAPES FOR TANGENT
AND CURVED TESTS

TANGENT TEST



ΔT_B (ABOVE STRESS FREE) = 139°F (AVG.)
 AXIAL FORCE PER RAIL = 134 TONNES

5° CURVED TEST



ΔT_B (ABOVE STRESS FREE) = 110°F (AVG.)
 AXIAL FORCE PER RAIL = 108 TONNES

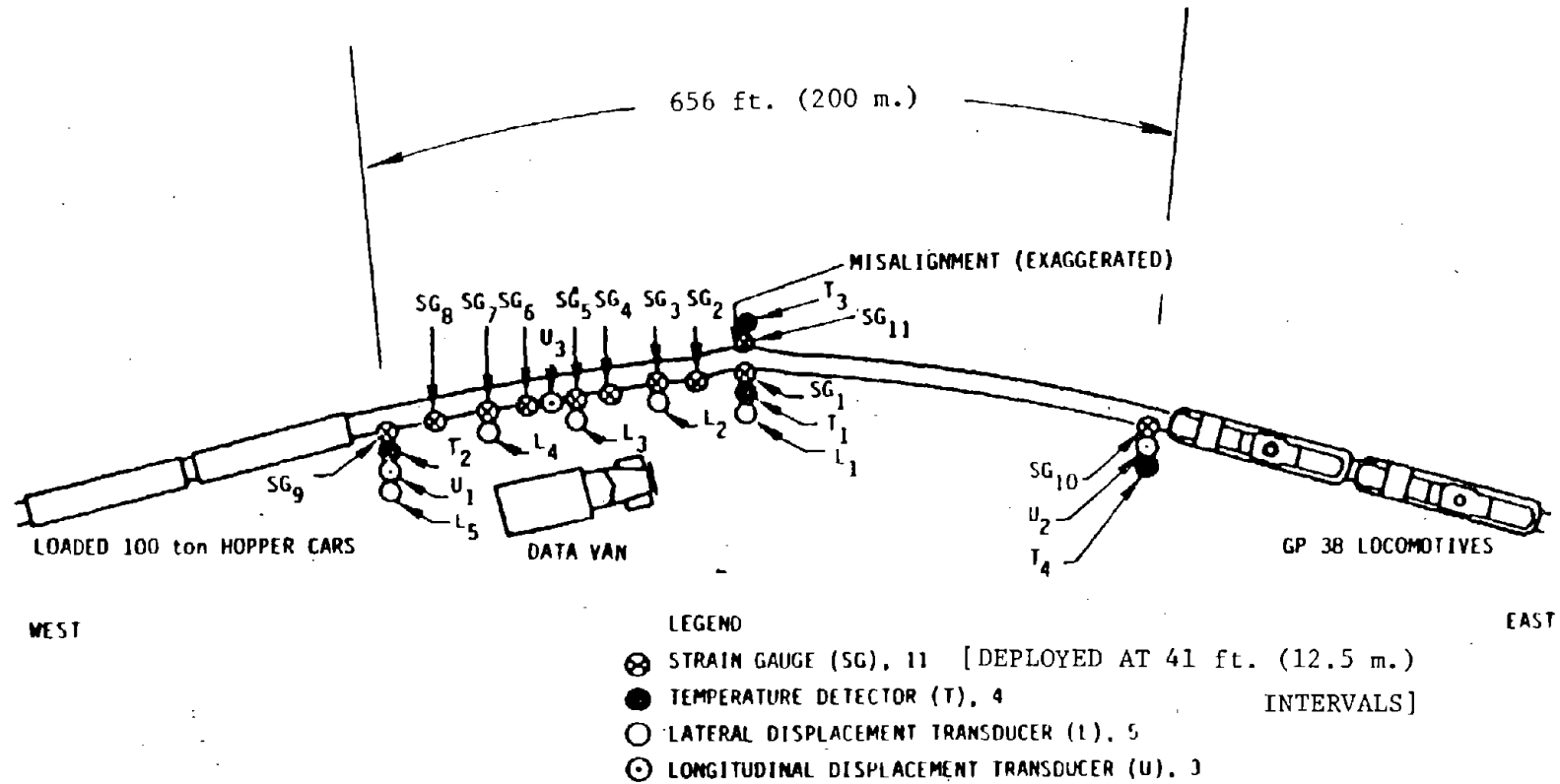


FIG. 4 - CURVED TRACK INSTRUMENTATION

(lateral) movements in the breathing zone, i.e., zone adjacent to the buckling zone. Again, all the instrument outputs were recorded on a Datalogger. As in the tangent track, X-Y plotters were employed to obtain the response characteristics and the test track end stiffness.

Test Procedure: De-stressing, misalignment installation, rail heating, etc., were all carried out in the same manner as for the tangent track. An initial imperfection of 1.5 in. (38 mm) over 36.1 ft. (11 m) was installed, and force-deflection data were collected to compute the lateral resistance. The track buckled in Shape I mode (see Table 3). Typical outputs from the datalogger just before and after buckling are shown in Table 4. The rate of heating is shown in Figure 5.

TABLE 4 - TYPICAL OUTPUT FROM DATALOGGER
(CURVED TRACK)

023 *	0.86823	INS.
022 *	0.56309	INS.
021 *	3.13424	INS.
020 *	-0.63165	INS.
019 *	16.1829	INS.
018 *	0.96137	INS.
017 *	0.83570	INS.
016 *	0.89856	INS.
015	185.449	DEG-F
014	180.001	DEG-F
013	195.133	DEG-F
012	187.717	DEG-F
011	-65.3619	K TON
010	-57.6432	K TON
009	-89.6740	K TON
008	-88.2887	K TON
007	-87.4244	K TON
006	-93.2333	K TON
005	-50.6234	K TON
004	-85.8397	K TON
003	-73.9369	K TON
002	-62.1856	K TON
001	-74.8024	K TON
12-21-87	JUN 26, 1991	
CURVE		

L 5	023 *	0.86823	INS.
L 4	022 *	0.56309	INS.
L 3	021 *	3.13424	INS.
L 2	020 *	-0.63165	INS.
L 1	019 *	16.1829	INS.
U 3	018 *	0.96137	INS.
U 2	017 *	0.83570	INS.
U 1	016 *	0.89856	INS.
T 4	015	185.449	DEG-F
T 3	014	180.001	DEG-F
T 2	013	195.133	DEG-F
T 1	012	187.717	DEG-F
SG 11	011	-65.3619	K TON
SG 10	010	-57.6432	K TON
SG 9	009	-89.6740	K TON
SG 8	008	-88.2887	K TON
SG 7	007	-87.4244	K TON
SG 6	006	-93.2333	K TON
SG 5	005	-50.6234	K TON
SG 4	004	-85.8397	K TON
SG 3	003	-73.9369	K TON
SG 2	002	-62.1856	K TON
SG 1	001	-74.8024	K TON
	12-21-87	JUN 26, 1991	
	CURVE		

BEFORE BUCKLING

AFTER BUCKLING

* TO BE ADJUSTED FOR INITIAL VALUES

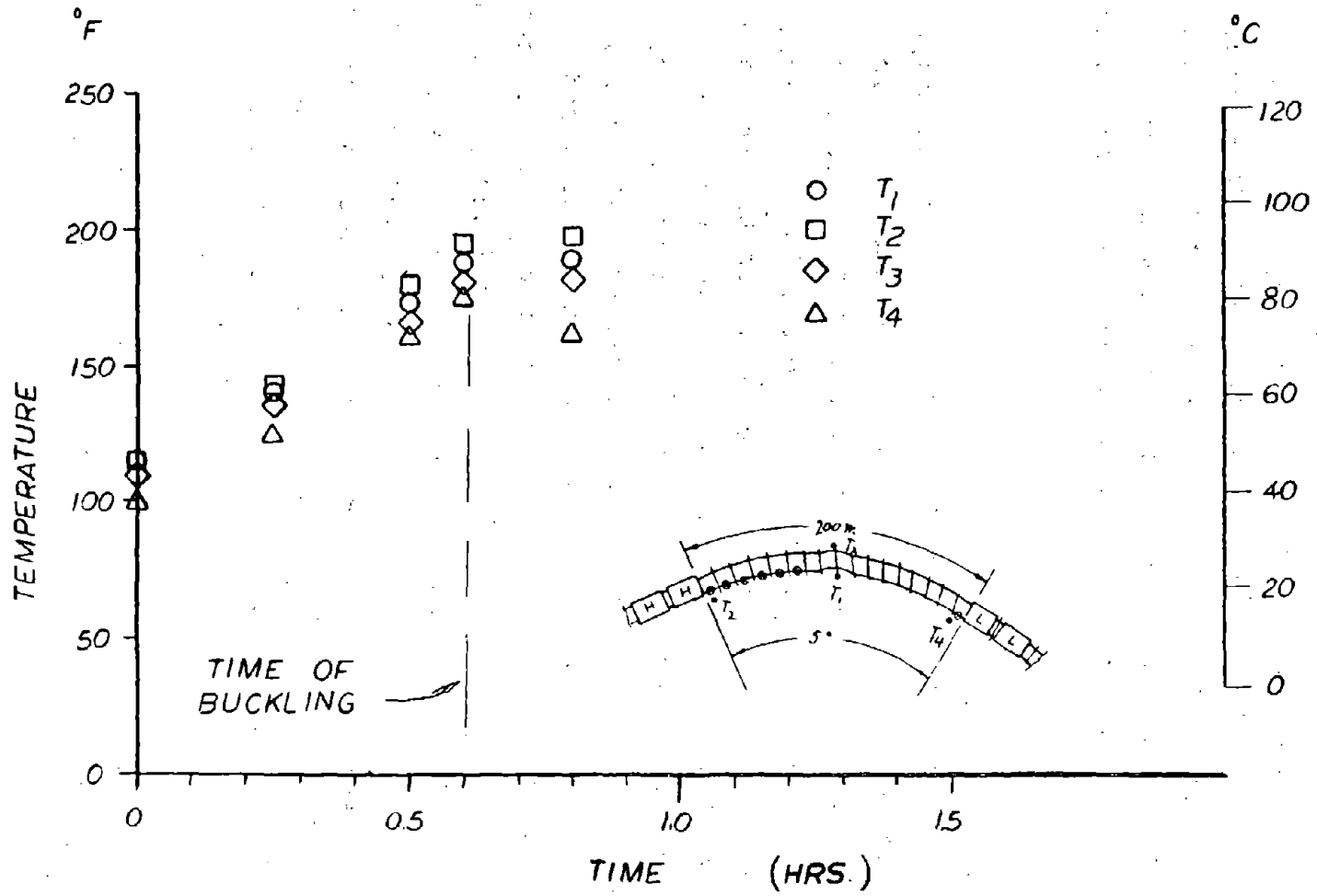


FIG. 5 - CURVED TRACK HEATING RATE

4. TRACK PARAMETERS

The quantitative determination of relevant track parameters for use in the analyses constituted an important part of the tests. No attempt was made to control parameters artificially in the tests, excepting for the initial misalignment. This resulted in a realistic response of the test track and representative data for the service track. In the following, the key parameters required for use in the theory as given in Section 5 are briefly discussed.

4.1 STRESS-FREE TEMPERATURE

Stress-free or neutral temperature is defined as the temperature at which no resultant longitudinal force acts in the rail. Ideally, this would be the rail temperature at the instant of closing the joints after the de-stressing operation. In practice, however, joint closing and re-anchoring takes finite time and the rail temperature changes during this period. The method of determining the stress-free temperature in the test was to plot the rail force (as read by the strain gauges) against the rail temperature, as shown in Figure 6 for the tangent track and Figure 7 for the curved track, and extrapolate the graph to cut the temperature axis. In these figures, SG_2 readings (the strain gauge situated at 41 ft. or 12.5 m from the center) were used rather than SG_1 which was located in the misalignment zone. The logic in fitting the data by a straight line in Figures 6 and 7 is that, after re-anchoring for small levels of force, the relationship between the force and the temperature increase is linear.

As seen from Figures 6 and 7, the stress-free temperature works out to be 71.3°F (21.8°C) for the tangent and 72.3°F (22.4°C) for the curved track.

4.2 INITIAL MISALIGNMENT

The purpose of the initial misalignment was to assess the track buckling sensitivity to imperfections. It would also

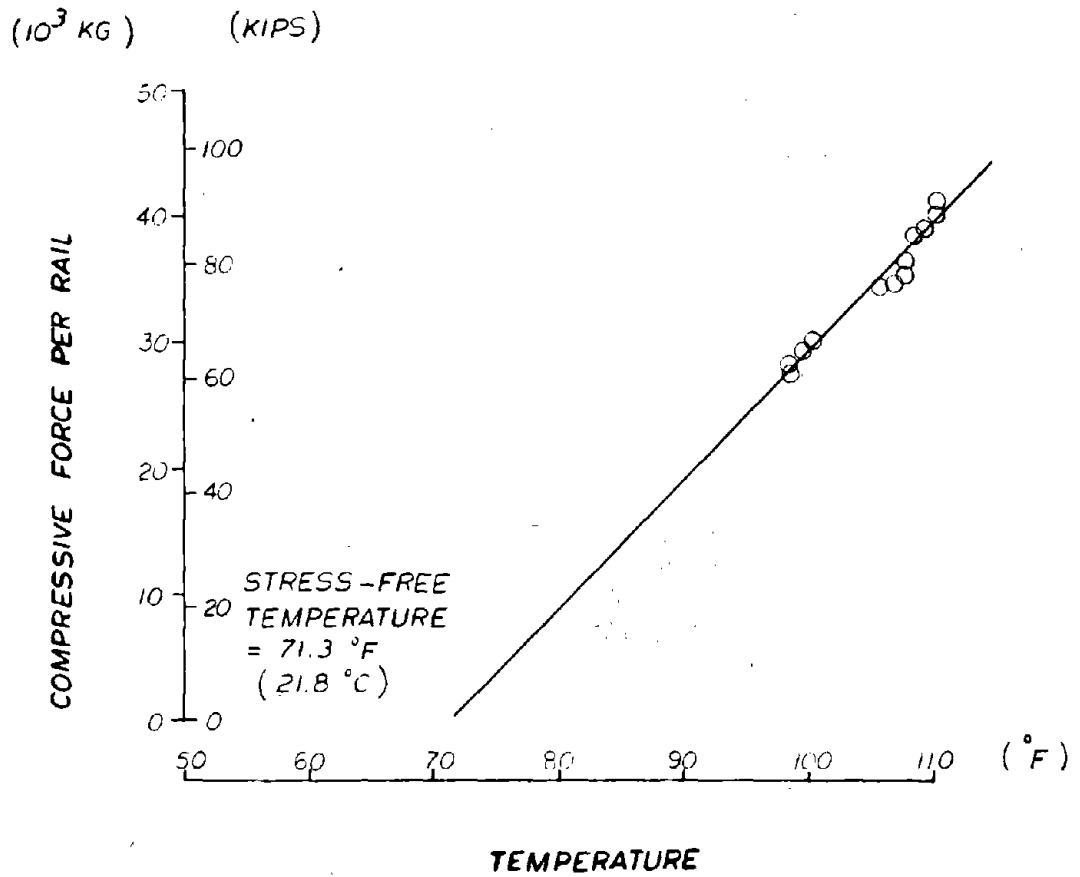


FIG. 6 - STRESS-FREE TEMPERATURE (TANGENT TRACK)

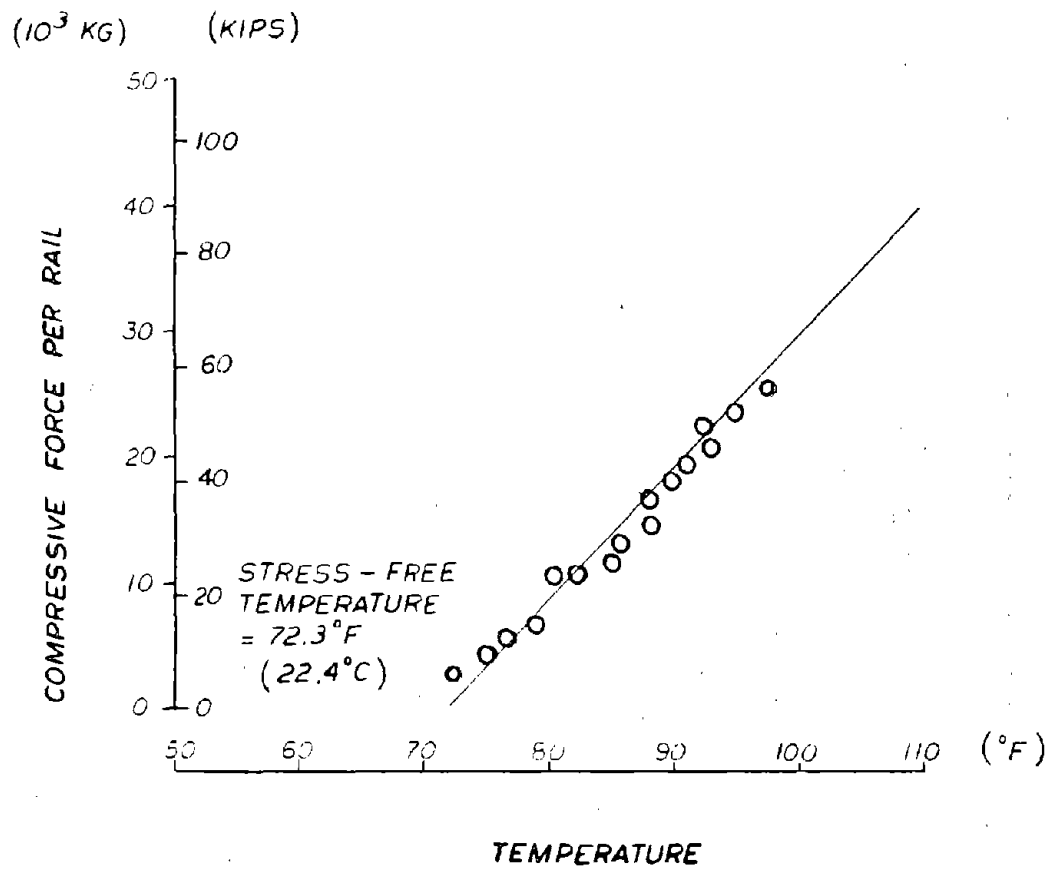


FIG. 7 - STRESS-FREE TEMPERATURE (CURVED TRACK)

precipitate buckling to occur at a chosen place (center) and facilitate the determination of the track lateral resistance. As stated earlier, the misalignment was set by applying a lateral force through a hydraulic jack, connected to a reacting bulldozer (Figure 2).

Tangent Track: For the purpose of computing the lateral resistance, the lateral deflections at $x=0$, $x=x_1$, and $x=x_2$ were recorded at different load levels, as shown in Figure 8.

The final misalignment shape at the commencement of the buckling test was measured relative to a stringline and also shown in Figure 8. The amplitude of the misalignment is about 1.61 in. (41 mm), within a chord length of 36.1 ft. (11 m).

Curved Track: The setting of misalignment posed certain problems. The bulldozer had to be placed in a ditch and considerable effort was required to apply a purely horizontal force, working against a 2.5" superelevation. In addition, it was found that at high lateral load levels, the reacting bulldozer did not provide adequate restraint.

The lateral deflection and force measurements taken during the misalignment setting for the curve are shown in Figure 9. Also shown is the final misalignment shape, with an amplitude of 1.5 in. (38 mm) over a length of 36.1 ft. (11 m).

4.3 LATERAL RESISTANCE

Existing methods for determination of track lateral resistance rely on pulling a single or a panel of ties. Single tie tests are not suitable, in general, because of tie-to-tie variation in ballast conditions and discrete panel tests are also unsuitable for service track as they involve cutting the rails. No convenient method of measuring lateral resistance of service tracks exists in practice. Therefore, the following methods have been developed for the determination of track lateral resistance for the buckling test.

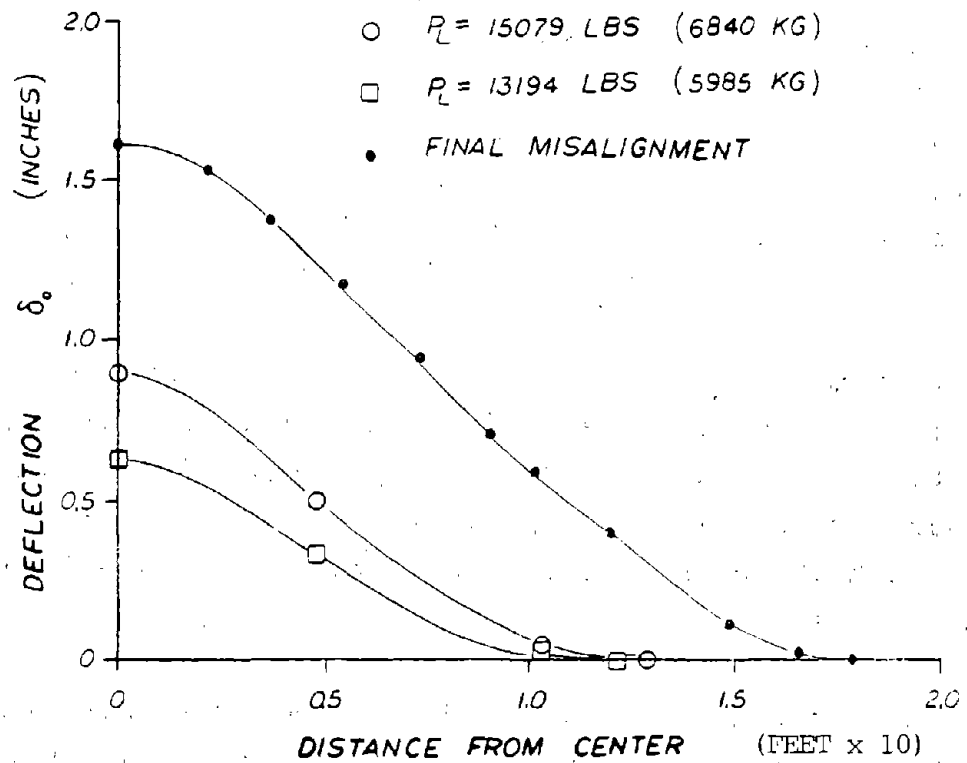


FIG. 8 - MISALIGNMENT SETTING (TANGENT TRACK)

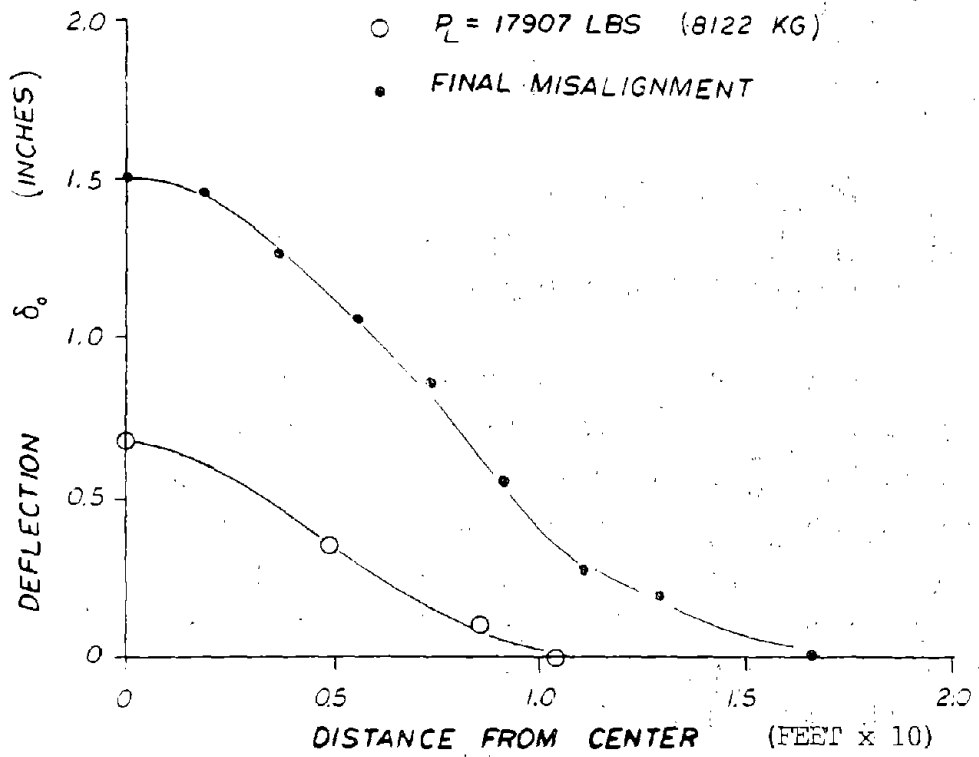


FIG. 9 - MISALIGNMENT SETTING (CURVED TRACK)

Tangent Track

Method 1: Lateral Resistance Computation from Misalignment Setting

This method utilizes the track deflection-force data obtained in Section 3.1 while the initial imperfection is set by the application of a lateral force (Figure 2). We assume that the track behaves like a beam in bending in the lateral plane and that there is no compressive force in the rails when a lateral force P_L is applied at the origin. The differential equation describing this behavior is:

$$EI w'''' = P_L \delta(0) - F(w) \quad (i)$$

Here $\delta(0)$ is the Dirac delta function, EI is the flexural rigidity, $F(w)$ is the lateral resistance function, and the primes denote derivatives with respect to x .

$F(w)$ is generally a nonlinear function of w , as shown in Figure 2.2, and it attains the steady value F_0 when the rail deflection $w \geq \bar{w}$ (Figure 2.2). Since F_0 is an important parameter in the buckling analyses, Equation (i) will be used to determine F_0 . For this purpose, it is necessary to consider the response of the portion of the deformed track in which $w > \bar{w}$, hence $F = F_0$. Assuming the P_L is sufficiently large as to yield $w_3 \geq \bar{w}$, the four deflection values $w = w_i$ ($i=0,1,2,3$) at $x = x_i$, together with the two conditions at $x = 0$, viz., $w' = 0$, $w'' = P_L/2EI$, will determine the six unknowns, namely, EI , F_0 and the four integration constants appearing in the solution of Equation (i). The fact that an equivalent EI will also result from this method is useful as this value can be compared with the generally accepted value computed from the material and the section properties of the rails. The method requires measurement of the four deflections with good accuracy and an engineering judgment of \bar{w} . For an approximate determination of F_0 , w can be considered as small and ignored.

Method 2: Lateral Resistance from Post-Buckled Equilibrium Shape

This method uses the compressive force-deflection data of the buckled track. The differential equation for the tangent track can be shown as (see Section 5)

$$EI w'''' + \bar{P}(w'' + w_0'') = \pm F_0 \quad (ii)$$

Since the buckling deflections are large, it is justified to use the constant value F_0 for the resistance. The \pm signs are to account for the sign of w in the Shape III mode (see Section 5, Figure 15). Here, w_0'' is the second derivative of the initial misalignment in the track.

The compressive force \bar{P} is read from the strain gauges. (Gauge 2, which is in the buckled zone, is considered here rather than Gauge 1 at the center, as there is plastic yielding of the rail at the center. This is discussed later.) Equation (ii) is solved conveniently by the Fourier technique (see Section 5). To simplify computations, EI is assumed known in the analysis (although it does not have to be), and knowing \bar{P} , L_1 , L , w_{\max} (Figure 15) and using Eq. (ii), F_0 can be evaluated.

Curved Track

Method 1

We assume that there is no compressive force in the rails when the lateral force is applied. The differential equation is

$$EI \frac{w}{R^4} = P_L \delta(0) - F_0 \quad (iii)$$

where the dots denote the derivatives with respect to θ (Figure 15). As in the case of tangent track, Eq. (iii) can be integrated and from the lateral force-deflection data collected during the misalignment setting (Figure 9), one can evaluate F_0 .

Method 2

The buckled equilibrium equation for the track can be shown to be (Section 5)

$$\frac{EI \bar{w}''''}{R^4} + \frac{\bar{P} \bar{w}''}{R^2} = -F_0 + \frac{\bar{P}}{R} - \frac{\bar{P} \bar{w}_0''}{R^2} \quad (iv)$$

The compressive force \bar{P} in the buckled zone is read from the strain gauges. The differential equation (iv) is conveniently solved by the Fourier technique and F_0 can be evaluated in terms of the maximum deflection and \bar{P} .

Numerical Results

For the tangent track, the following results are obtained from the data in Figure 8. It is assumed that $\bar{w} = 0$ in Method 1.

P_L lb (kg)	EI lb-in ² (kg-m ²)	F_0 lb/in (kg/m)
13194 (5985)	.112 x 10 ¹⁰ (.328x10 ⁶)	57.6 (1031)
15079 (6840)	.102 x 10 ¹⁰ (.299x10 ⁶)	63.0 (1127)

The value of EI is about 20 percent higher than the value obtained from material and sectional properties of rails. This may be attributed to the influence of torsional resistance present in the track. The average value of lateral resistance is 60.3 lb/in (1078 kg/m).

In Method 2, the data used for the tangent track are $EI = .1 \times 10^{10}$ lb-in² = .293 x 10⁶ kg/m², $L = 49.5$ ft. = 15.1 m, $L_1 = 20.7$ ft. = 6.3 m, $L_0 = 18.04$ ft. = 5.5 m, $w_{\max} = 25$ in. = .635 m, $\epsilon_0 = 1.61$ in. = .041 m, $\bar{P} = 69.2$ tons or 138,380 lb. (interpolated from SG_2 and SG_3) for the two rails. F_0 is found to be 48.3 lb/in (865 kg/m). The value is reasonably close to that of Method 1, when one considers the variable nature of revenue service tracks.

For the curved track, only one set of readings at $P_L = 17907$ lbs (8122 kg) (Figure 9) is believed to be reliable for calculating the lateral resistance. This has yielded the following result

P_L lb (kg)	EI lb-in ² (kg-m ²)	F_O lb/in (kg/m)
17907 (8122)	$.115 \times 10^{10}$ ($.337 \times 10^6$)	99.4 (1779)

The EI value obtained is reasonable. The lateral resistance $F_O = 99.4$ lb/inch = 1779 kg/m is considerably higher than expected.

In Method 2 for the curved track, the data used are $EI = .1 \times 10^{10}$ lb-in² = $.293 \times 10^6$ kg/m², $E = 37.7$ ft. = 11.5 m, $L_O = 18.04$ ft. = 5.5 m, $\delta_O = 1.5$ in. = .038 m, $w_{max} = 13.4$ in. = 0.34 m, $\bar{P} = 138.5$ tons or 276,980 lb. for the two rails. The lateral resistance is found to be 67.1 lb/in. (1200 kg/m).

The difference in the obtained lateral resistance values for the tangent and the curve may be attributable to the wider shoulder width and more cemented ballast on the curve. For analysis purposes, the average values of 54.3 lb/in (972 kg/m) and 83.3 lb/in (1490 kg/m) for the tangent and curve, respectively, were used.

4.4 LONGITUDINAL RESISTANCE

Longitudinal resistance is the resistance experienced by rails as they move in the longitudinal direction. Usually rail anchors are tight, and ties also move along with the rails. The resistance offered by the ballast to ties will then be the longitudinal resistance. In some situations, the anchors may be loose or missing, resulting in rail slippage over the ties, and hence, results in reduced resistance.

The mathematical representation of the longitudinal resistance is generally of the form $f(u) = f_0 \tanh \mu u$ [6]. Here, f_0 is the constant value reached for large longitudinal displacement, u , and μ is a stiffness parameter.

There are no simple ways of determining the longitudinal resistance of tracks in service. In the buckling experiment, advantage can be taken of the rail force levels indicated by the strain gauges. The longitudinal equilibrium equation in the zone adjacent to the buckled zone can be shown as (Figure 14)

$$\frac{dP}{dx} = f(u) \quad (v)$$

For large u , $f(u)$ being $\pm f_0$, the rail force gradient is a direct measure of f_0 . The following methods are used to determine this gradient.

Method 1

If we consider the prebuckling longitudinal displacements, the largest movement occurs at the ends of the test section due to finite stiffness at the ends. For the tangent track (Figure 10),

$$f_0 = 2(SG_7 - SG_9)/25 = 89.4 \text{ lb/in (1600 kg/m)}$$

Similarly, for the curved track (Figure 11), SG_6 and SG_8 values indicate:

$$f_0 = 2(SG_6 - SG_8)/25 = 71.5 \text{ lb/in (1280 kg/m)}$$

Method 2

In this method, we consider the post-buckling longitudinal movement of the rails. The largest movement occurs near the ends of the buckled zone. From Figure 10, for the tangent track:

$$f_0 = 2(SG_4 - SG_2)/25 = 49.2 \text{ lb/in (880 kg/m)}$$

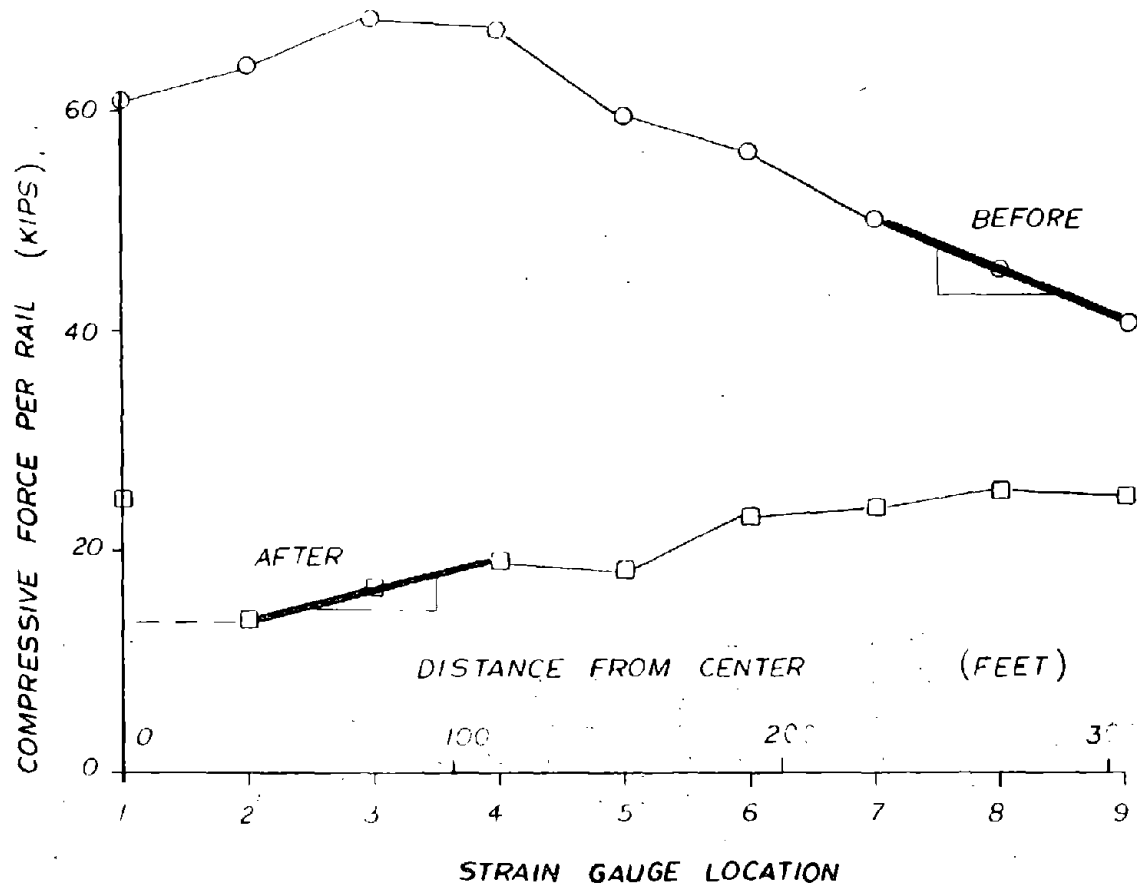


FIG. 10 - LONGITUDINAL FORCE DISTRIBUTION (TANGENT TRACK)

For the curved track (Figure 11):

$$f_o = 2(SG_6 - SG_8)/25 = 102.8 \text{ lb/in (1840 kg/m)}$$

The two methods yielded significantly different results, which can be attributed to the variable nature of the track. The resistance may also be dependent on the direction of movement. It is also nonlinear with respect to the longitudinal movement.

4.5 END STIFFNESS

The end stiffness at the junction between the heated test rail and the unheated cold rail outside the test zone is an important parameter in the analysis of finite tracks. Figures 12 and 13 show the relationship between SG_9 and U_1 for the tangent and the curved tracks, respectively.

In the tests, the longitudinal transducers were connected late (after the de-stressing operations) when there were already some movement due to the temperature increase. The data plotted in Figures 12 and 13 were not corrected for the initial displacement. It is believed that with this correction, the graph would intercept the force axis nearer the origin. The graph is linearized and the stiffness works out to be

$$k = 1.12 \times 10^6 \text{ lb/in (} 2 \times 10^7 \text{ kg/m)}$$

both for the tangent and curved tracks.

4.6 SUMMARY

1. A summary of the track parameters determined by the foregoing analyses is presented in Table 1 for both the tangent and the curved tracks. The final resistance values given are the average values obtained from Methods 1 and 2. This averaging must be done to accommodate the variable nature of the track characteristics.

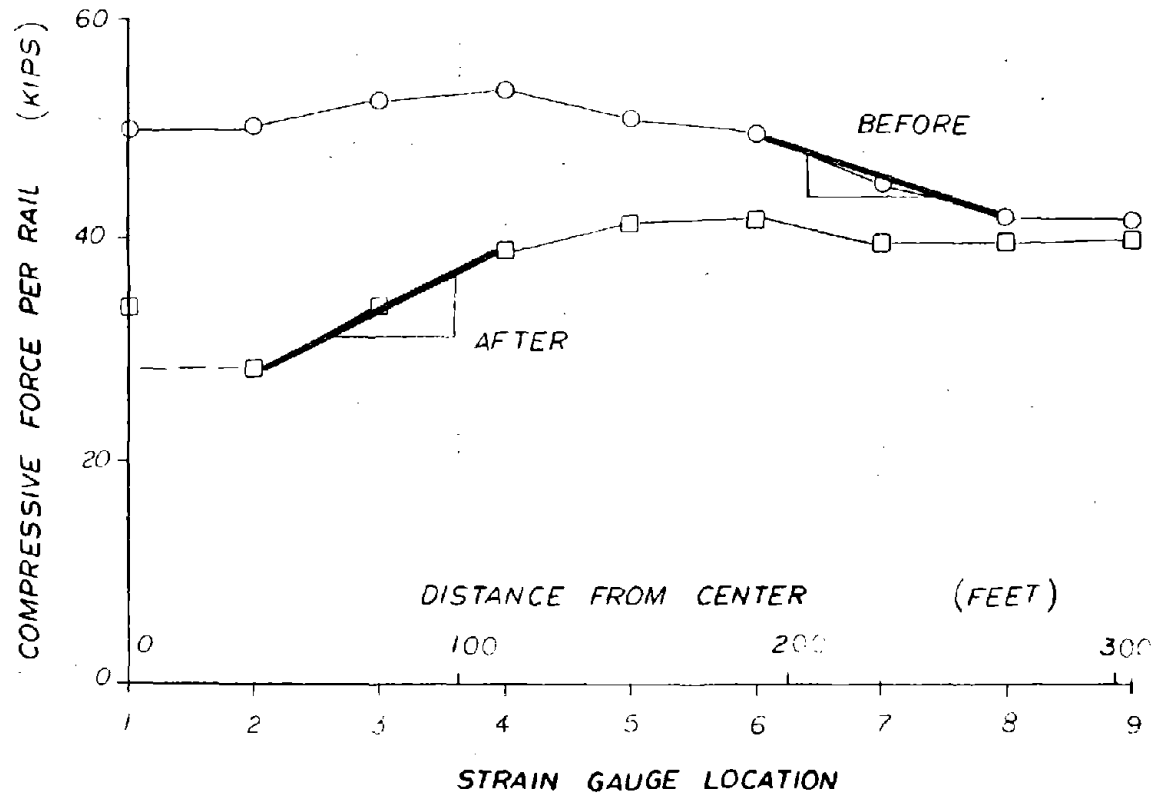


FIG. 11 - LONGITUDINAL FORCE DISTRIBUTION (CURVED TRACK)

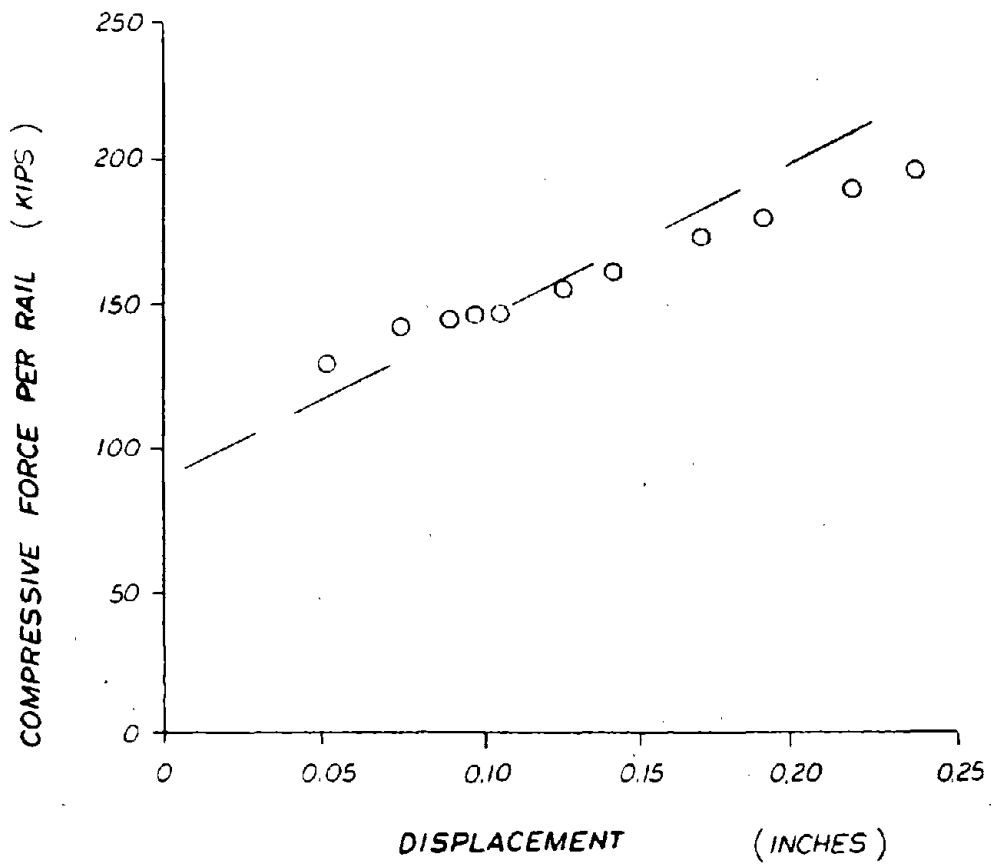


FIG. 12 - END STIFFNESS COMPUTATION (TANGENT TRACK)

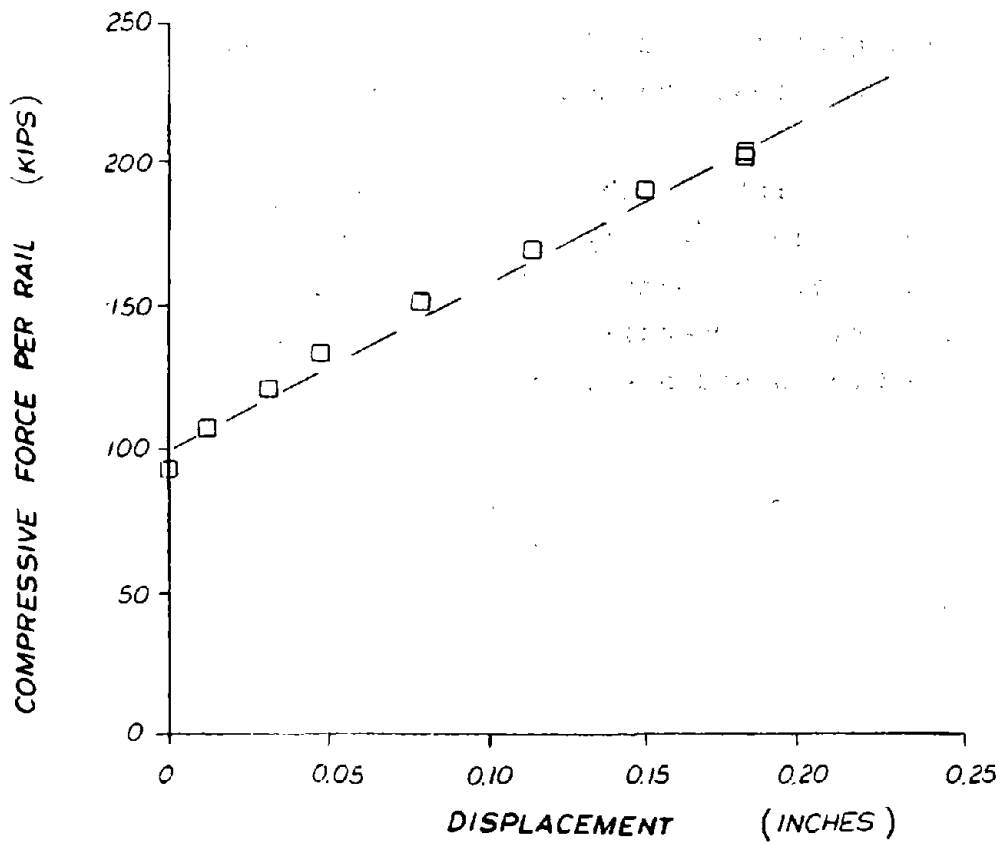


FIG. 13 - END STIFFNESS COMPUTATION (CURVED TRACK)

2. The track, even after tamping, showed a lateral resistance of 54 lb/in and 83 lb/in for the tangent and curve, respectively.

3. The longitudinal resistance of the track is high (70 - 87 lb/in) even when every other tie is box anchored. The resistance seems to be unequal in the two directions.

4. The apparent flexural rigidity EI of the track is about 20 percent higher than the usually assumed value.

5. The end stiffness obtained between the cold and hot junctions is about 1.12×10^6 lb/in. This seems reasonable, when compared with previous data obtained at the Chattanooga, TN, buckling test site (Appendix 2). British Rail test track with end concrete blocks had a stiffness of one order of magnitude higher [14].

5. GENERAL THEORY

In order to analyze and interpret the results of the buckling tests, a general theory accounting for the finite track length, the finite stiffness and the prebuckling longitudinal movements is given below.

The initial (prebuckling) displacement is sketched in Figure 14. It can be shown that the end effect is felt up to a distance, l_s , where

$$l_s = \left(\frac{AE}{k} \right) \left[\sqrt{1 + \frac{2k\alpha T}{f_0}} - 1 \right] \quad (1)$$

When buckling occurs there will be a drop in the rail force in the buckled zone. This will result in some longitudinal movement of a part of the adjoining region towards the buckle. The force will be redistributed as shown in Figure 14. It is clear that the peak of the force curve occurs at the point of zero longitudinal displacement.

5.1 EQUATIONS FOR THE BREATHING ZONE

It is convenient to divide the adjoining zone into two regions: $L \leq x \leq l_1$, and $l_1 \leq x \leq l$. Let U_1 and U_2 be the net longitudinal displacements in the two regions after buckling. The differential equations are:

$$U_1'' = - f_0/EA \text{ hence } U_1 = - \frac{f_0 x^2}{2EA} + C_1 x + C_2 \quad (2)$$

$$U_2'' = + f_0/EA \text{ hence } U_2 = + \frac{f_0 x^2}{2EA} + C_3 x + C_4 \quad (3)$$

It has been shown in an earlier work [6], that, u , the displacement in the buckled zone $|x| < L$ can be expressed in terms of \bar{P} and w , the lateral displacement. Also,

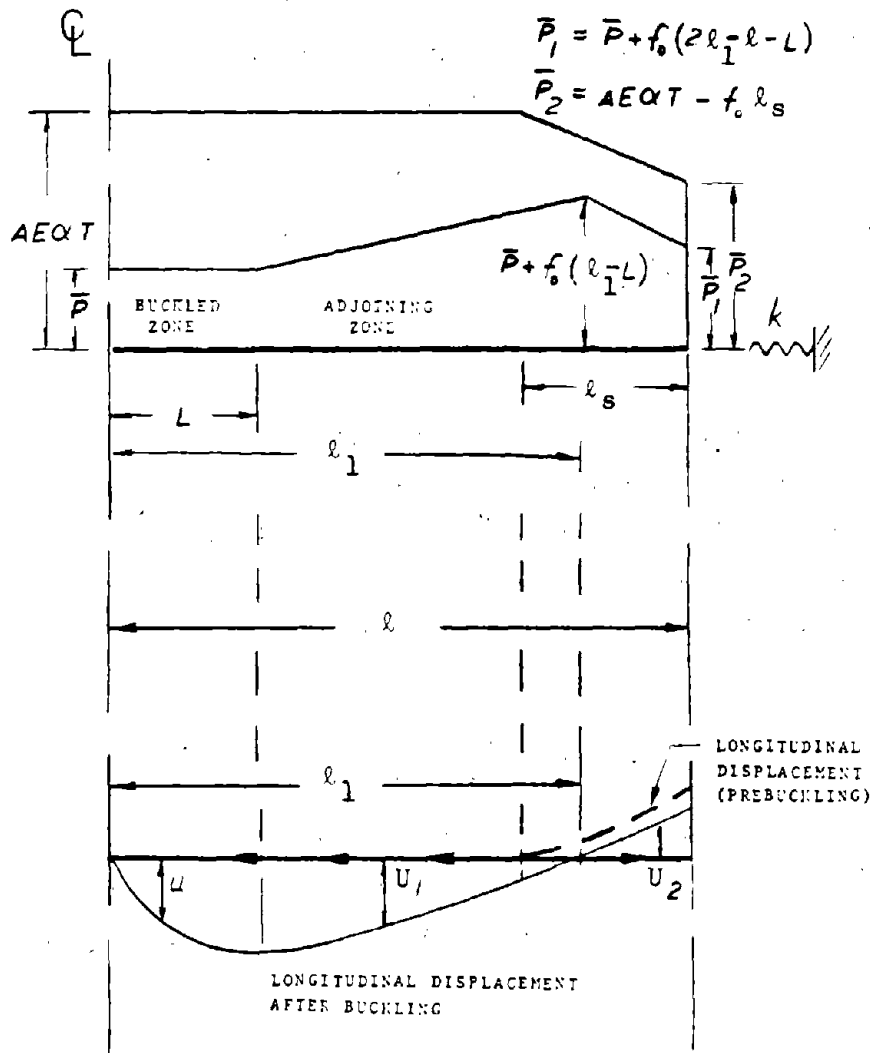


FIG. 14 - ILLUSTRATION OF THE EFFECTS OF FINITE TRACK LENGTH, l , AND END STIFFNESS, k .

$$u' \Big|_{x=L} = - \frac{\bar{P}}{EA} + \alpha T \quad (4)$$

$$u \Big|_{x=L} = - \frac{\bar{P}L}{EA} + \alpha TL - z \quad (5)$$

where

$$z = \int_0^L \left(\frac{w'^2}{2} + w'w'_0 \right) dx \quad (6)$$

For an assumed value of L , \bar{P} is determined from the transcendental equations as shown later. There are now six unknowns in the problem: $C_1, C_2, C_3, C_4, \ell_1$ and T , the temperature. These are determined from the following continuity and end conditions:

$$U_1 \Big|_{x=\ell_1} = 0 \quad (7.1)$$

$$U_2 \Big|_{x=\ell_1} = 0 \quad (7.2)$$

$$U_1' \Big|_{x=\ell_1} = U_2' \Big|_{x=\ell_1} \quad (7.3)$$

$$U_1 \Big|_{x=L} = u \Big|_{x=L} \quad (7.4)$$

$$U_1' \Big|_{x=L} = u' \Big|_{x=L} \quad (7.5)$$

$$\bar{P} + f_0(2\ell_1 - L) = kU_2 \Big|_{x=\ell} \quad (7.6)$$

Equations 7.1-7.3 represent the continuity between region 1 and region 2. Equations 7.4 and 7.5 represent the continuity between the buckled zone and region 1. Equation 7.6 gives the end stiffness condition. After some lengthy algebra, it can be shown that the final equation for the determination of ℓ_1 is given by:

$$\begin{aligned}
& - 2(\ell_1/\ell)^3 + \left[3 + \frac{4AE}{k\ell} \right] (\ell_1/\ell)^2 + \left[-1 + \left(\frac{L}{\ell} \right)^2 \right. \\
& \left. - \frac{2AE}{k\ell} (1 + L/\ell) + \frac{AE}{f_o \ell^2} \left(\frac{2}{k} + z \right) \right] (\ell_1/\ell) \\
& - \left[(L/\ell)^2 + AEZ/(f_o \ell^2) \right] = 0 \quad (8)
\end{aligned}$$

It is not difficult to show that the foregoing cubic equation has only one positive root for $\ell_1 < \ell$. The final equation for the temperature T , is given by:

$$T = \frac{f_o (\ell_1 - L)^2}{2EA\alpha\ell_1} + \frac{\bar{P}}{AE\alpha} + \frac{z}{\ell_1\alpha} \quad (9)$$

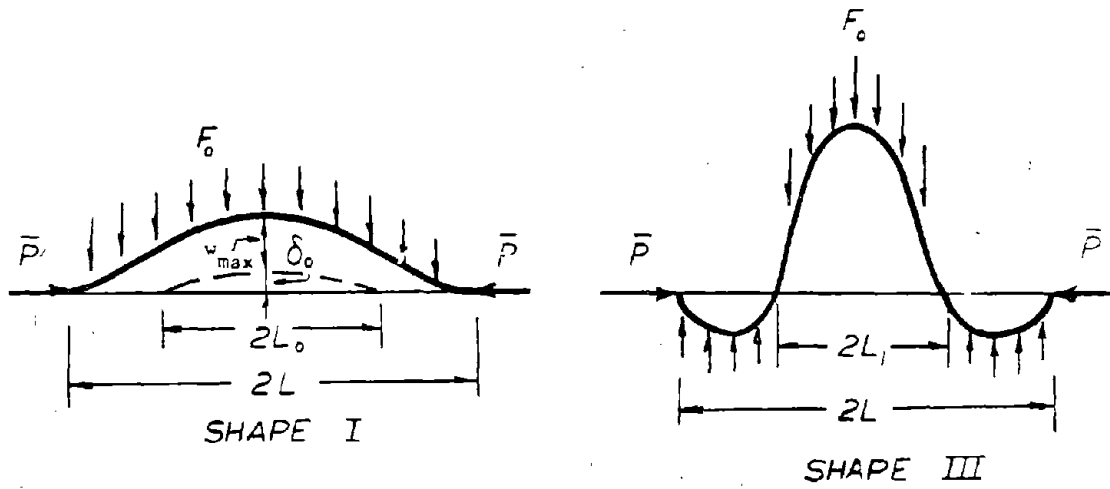
For the special case where the end stiffness, k , approaches infinity, ℓ_1 approaches ℓ and equation 9 reduces to the previously derived equation for finite tracks [15]. The equation for curved track is similar (with appropriate changes in z).

5.2 EQUATIONS FOR BUCKLED ZONE (TANGENT TRACK)

The following equations are derived under the usual assumptions for the buckles zone, i.e., the lateral resistance $F(w) = F_o$, constant, and the longitudinal resistance $f_o = 0$ (see Reference 6). Both Shape I and Shape III modes (see Figure 15) will be considered for tangent track because of the mode transformation taking place from I to III, as explained later. The track, at the instant of buckling, was in Shape I although the final post-buckled shape was III.

The initial track imperfection is assumed to be sinusoidal:

$$w_o(x) = \delta_o \cos \left(\frac{\pi x}{2L_o} \right) \quad (10)$$



TANGENT TRACK

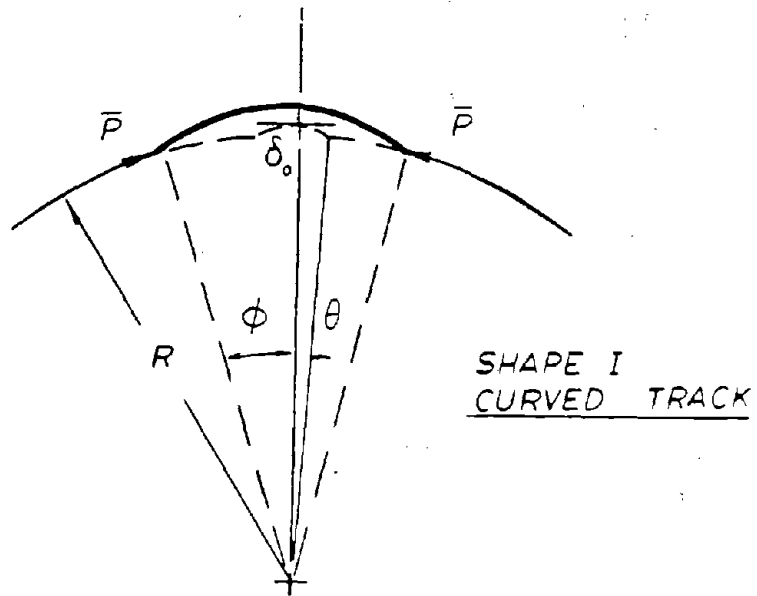


FIG. 15 - BUCKLING MODE SHAPES

SHAPE I

The differential equation is:

$$EI w'''' + \bar{P} w'' = - F_0 - \bar{P} w_0'' \quad (11)$$

The boundary conditions are as follows:

$$\text{at } x = 0 \quad w' = w''' = 0 \quad (11.1)$$

$$\text{at } x = \pm L \quad w = w' = w'' = 0 \quad (11.2)$$

Let

$$w(x) = \sum_{1,3,5,\dots}^{\infty} A_m \cos\left(\frac{m\pi x}{2L}\right) \quad (12)$$

$$F_0(x) = \sum_{1,3,5,\dots}^{\infty} a_m \cos\left(\frac{m\pi x}{2L}\right) \quad (12.1)$$

$$w_0'' = \sum_{1,3,5}^{\infty} b_m \cos\left(\frac{m\pi x}{2L}\right) \quad (12.2)$$

By Fourier analysis

$$a_m = \frac{4F_0}{m\pi} \sin\left(\frac{m\pi}{2}\right) \quad (12.3)$$

$$\begin{aligned} b_m &= \frac{2}{L} \int_0^L w_0'' \cos\left(\frac{m\pi x}{2L}\right) dx \\ &= - \frac{\pi \delta_0 (L/L_0) \cos\left(\frac{m\pi L_0}{2L}\right)}{\left(L^2 - L_0^2 m^2\right)} \text{ for } L_0 < L \end{aligned} \quad (12.4)$$

$$= - \frac{\pi \delta_0 m \cos\left(\frac{\pi L}{2L_0}\right) \sin\left(\frac{m\pi}{2}\right)}{\left(m^2 L_0^2 - L^2\right)} \text{ for } L_0 > L \quad (12.5)$$

also

$$A_m = \frac{-\left(a_m + \bar{P} b_m\right)}{\left[EI\left(\frac{m\pi}{2L}\right)^4 - \bar{P}\left(\frac{m\pi}{2L}\right)^2\right]} \quad (12.6)$$

The complete solution is obtained by stipulating that

$$w' \Big|_{x=L} = - \sum_{1,3,5,\dots}^{\infty} A_m \left(\frac{m\pi}{2L}\right) \sin\left(\frac{m\pi}{2}\right) = 0 \quad (12.7)$$

which gives

$$\sum_{1,3,5,\dots}^{\infty} \left[\frac{4F_o L^3}{EI m \pi} \sin \frac{m\pi}{2} - \frac{\beta \pi (\delta_o / L_o) \cos\left(\frac{m\pi L_o}{2L}\right)}{\left(1 - \frac{m^2 L_o^2}{L^2}\right)} \right] \sin\left(\frac{m\pi}{2}\right) \frac{1}{\left(\frac{m\pi}{2}\right) \left[\left(\frac{m\pi}{2}\right)^2 - \beta\right]} = 0 \quad (13)$$

Equation 13 determines β , the smallest root of which occurs between $(\pi/2)^2$ and $(3\pi/2)^2$.

$$\text{Here } \beta = \bar{P}L^2/EI \quad (13.1)$$

The value of Z required in the temperature equation (9) is calculated from:

$$\begin{aligned} Z &= \int_0^L \left(\frac{w'^2}{2} + w'w_o' \right) dx, \text{ which after integration by parts becomes:} \\ &= \int_0^L \left(\frac{w'^2}{2} - ww_o'' \right) dx \\ &= \frac{L}{2} \left[1/2 \sum_{\text{odd}}^{\infty} A_m^2 \left(\frac{m\pi}{2L}\right)^2 - \sum_{\text{odd}}^{\infty} A_m b_m \right] \end{aligned} \quad (14)$$

SHAPE III

In computing the post-buckling response (determined by Shape III), it is convenient to neglect the initial imperfections, as the latter are very small compared to the former and do not significantly influence the response beyond the safe temperature. The differential equation is

$$EI w'''' + \bar{P} w'' = - F(x) \quad (15)$$

From Figure 15, it is clear that

$$\left. \begin{aligned} F(x) &= + F_0 \text{ for } -L_1 < |x| < L_1 \\ &= - F_0 \text{ for } L_1 < |x| < L \end{aligned} \right\} \quad (15.1)$$

The boundary conditions are the same as Shape I, equations 11.1 and 11.2. In addition, there is the requirement that

$$w(L_1) = 0 \quad (15.2)$$

Writing w and $F(x)$ as

$$w(x) = \sum_{1,3,5,\dots}^{\infty} A_m \cos\left(\frac{m\pi x}{2L}\right) \quad (16)$$

$$F(x) = \sum_{1,3,5,\dots}^{\infty} a_m \cos\left(\frac{m\pi x}{2L}\right) \quad (16.1)$$

we find that

$$a_m = \frac{4F_0}{m\pi} \left[2 \sin\left(\frac{m\pi t}{2}\right) - \sin\left(\frac{m\pi}{2}\right) \right] \quad (16.2)$$

where $t = (L_1/L)$ and

$$A_m = - \frac{a_m}{\left[EI \left(\frac{m\pi}{2L}\right)^4 - \bar{P} \left(\frac{m\pi}{2L}\right)^2 \right]} \quad (16.3)$$

The boundary conditions together with equation 15.2 results in two transcendental equations for the determination of t and P . This work has been done before [6] and it has been found that

$$t = 0.385 \text{ and } \beta = \frac{\bar{P}L^2}{EI} = 57 \quad (17)$$

The expression for Z is:

$$Z = \left(\frac{L}{4}\right) \sum_{1,3,5,\dots}^{\infty} \left(\frac{m\pi}{2L}\right)^2 A_m^2 \quad (18)$$

5.3 EQUATIONS FOR BUCKLED ZONE (CURVED TRACK)

Initial misalignments are again assumed to be 'sinusoidal':

$$w_o(\theta) = \delta_o \cos\left(\frac{\pi\theta}{2\phi_o}\right), \text{ for } |\theta| < \phi_o \quad (19)$$

where δ_o is the amplitude or the offset and $2R\phi_o = 2L_o$ is the length over which the misalignment occurs. For symmetric buckling mode (see Fig. 15) the differential equation is:

$$\frac{EI}{R^4} \bar{w}'''' + \frac{\bar{P}w''}{R^2} = -F_o + \frac{\bar{P}}{R} - \frac{\bar{P}w_o''}{R^2} \quad (20)$$

$$\text{Let } w = \sum_{1,3,5,\dots}^{\infty} A_m \cos\left(\frac{m\pi\theta}{2\phi}\right) \quad (21)$$

$$\left(F_o - \frac{\bar{P}}{R}\right) = \left(F_o - \frac{\bar{P}}{R^2}\right) \sum_{1,3,5,\dots}^{\infty} a_m \cos\left(\frac{m\pi\theta}{2\phi}\right) \quad (21.1)$$

and

$$\frac{\bar{P}}{R^2} \bar{w}_o'' = \frac{\bar{P}}{R^2} \sum_{1,3,5}^{\infty} b_m \cos\left(\frac{m\pi\theta}{2\phi}\right) \quad (21.2)$$

The value of a_m is the same as in equation 12.3 whereas

$$\begin{aligned}
 b_m &= \frac{2}{\phi} \int_0^{\phi_0} \ddot{w}_0 \cos\left(\frac{m\pi\theta}{2\phi}\right) d\theta \\
 &= -\frac{\pi\delta_0(\phi/\phi_0) \cos\left(\frac{m\pi\phi_0}{2\phi}\right)}{(\phi^2 - \phi_0^2 m^2)} \quad (21.3)
 \end{aligned}$$

Also,

$$A_m = -\frac{[(F_0 - \bar{P}/R) a_m + (\bar{P}/R^2) b_m]}{\left[\frac{EI}{R^4} \left(\frac{m\pi}{2\phi}\right)^4 - \frac{\bar{P}}{R^2} \left(\frac{m\pi}{2\phi}\right)^2\right]} \quad (21.4)$$

The complete solution is obtained if it is stipulated that

$$\dot{w} \Big|_{\theta=\phi} = 0$$

that is,

$$\sum_{1,3,5}^{\infty} A_m m \sin\left(\frac{m\pi}{2}\right) = 0 \quad (21.5)$$

which determines \bar{P} or β , as before. The expression for Z in equation (9) is:

$$\begin{aligned}
 Z &= \int_0^{\phi} \left(\frac{w}{R} + \frac{\dot{w}^2}{2R^2} + \frac{\dot{w} \dot{w}_0}{R^2} \right) d\theta, \text{ which after integration by parts becomes:} \\
 &= \int_0^{\phi} \left(\frac{\dot{w}}{R} + \frac{\dot{w}^2}{2R^2} - \frac{w \ddot{w}_0}{R^2} \right) d\theta \\
 &= \sum_{1,3,5\dots}^{\infty} \left[\left(\frac{2\phi}{m\pi R}\right) \sin\left(\frac{m\pi}{2}\right) A_m + \left(\frac{m\pi}{R}\right)^2 \frac{1}{16\phi} A_m^2 - \frac{A_m b_m \phi}{2R^2} \right] \quad (21.6)
 \end{aligned}$$

The maximum deflection is

$$w_{\max} = \sum_{1,3,5,\dots}^{\infty} A_m \quad (21.7)$$

5.4 NUMERICAL SCHEME

All the relevant theoretical equations are easily programmable and are operational at TSC. A summary of the numerical scheme for the tangent track Shape I mode is given here. The scheme for the curved track is similar.

- (1) Select L varying from 3 to 15 meters in small increments, such as 0.25m
- (2) Determine β , for each L from the transcendental Eq. 13, using Newton Raphson method of iteration. Determine \bar{P} from Eq. 13.1
- (3) Compute a_m from Eq. 12.3, b_m from Eq. 12.4 or 12.5
- (4) Compute A_m from Eq. 12.6 and w_{\max} from Eq. 12
- (5) Compute Z from Eq. 14
- (6) Determine l_1 from Eq. 8. Accept the positive root $0 < l_1 < l$. If $l_1 > l$ set $l_1 = l$
- (7) Compute T from Eq. 9
- (8) Plot T vs w_{\max} and \bar{P} vs w_{\max}

Parametric studies have been carried out using the foregoing theory and the results will be presented in the forms of graphs and charts in a forthcoming publication [16].

6. TANGENT TRACK ANALYSES

The rail and the tangent track parameters summarized in Table 1 will be used in the general theory given in Section 5. The numerical results obtained from the theory will be compared with the test data recorded.

6.1 TEMPERATURE DEFLECTION RESPONSE

The theoretical buckling temperature (above neutral) was computed to be 136°F . The test value is slightly higher at 146°F indicating fairly good agreement. The buckled mode was the Shape III type. The maximum deflection obtained from Shape III theory is also in reasonable agreement with test value. Additional post-buckling measurements taken after the track buckled and as the heating continued, are also shown in Figure 16, which confirm the Shape III theoretical predictions. The theoretical safe temperature increase, ΔT_S is 78°F . It has not been possible to check this value from the test conducted.

It should be noted that Shape I analysis was used to predict the buckling temperature, while Shape III analysis was used for the final mode shape. This is justified because the track started to buckle in Shape I (due to Shape I imperfection), although its final shape was that of mode III. The transformation of the mode shape from I to III during buckling appears to be a common characteristic of the tangent track. The same phenomenon was noticed in the recent British Rail buckling tests in which a high-speed camera recorded the mode change.

6.2 RAIL FORCE-DEFLECTION RESPONSE

The theoretical rail compressive force values, as obtained in Shape I and III analyses, and the test results are plotted against the maximum central track deflection in Figure 17. Again, the test results agree better with Shape I theory before buckling and with Shape III theory after buckling, which further supports the contention that the mode change took place during buckling.

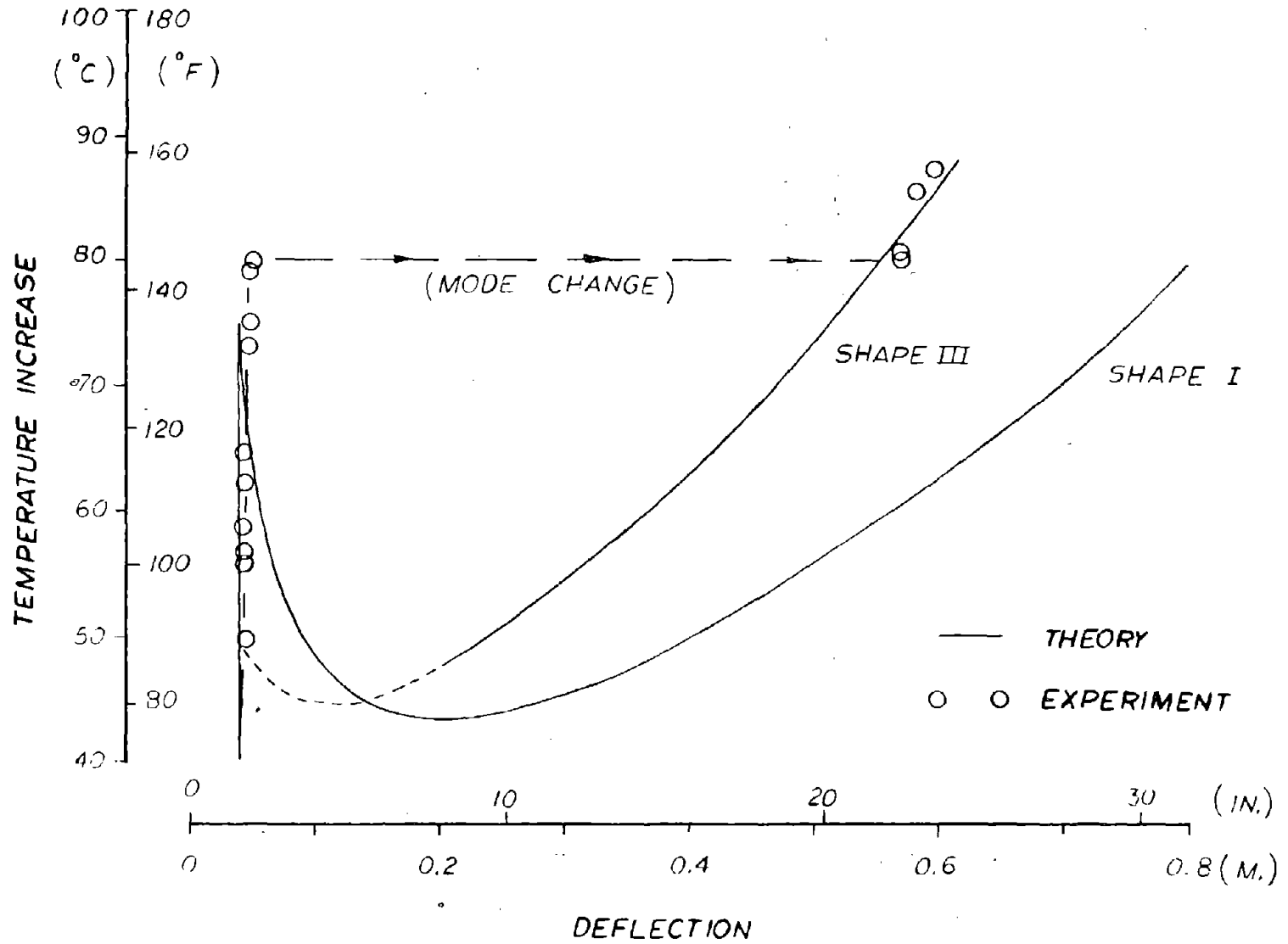


FIG. 16 - TEMPERATURE-DEFLECTION RESPONSE (TANGENT TRACK)

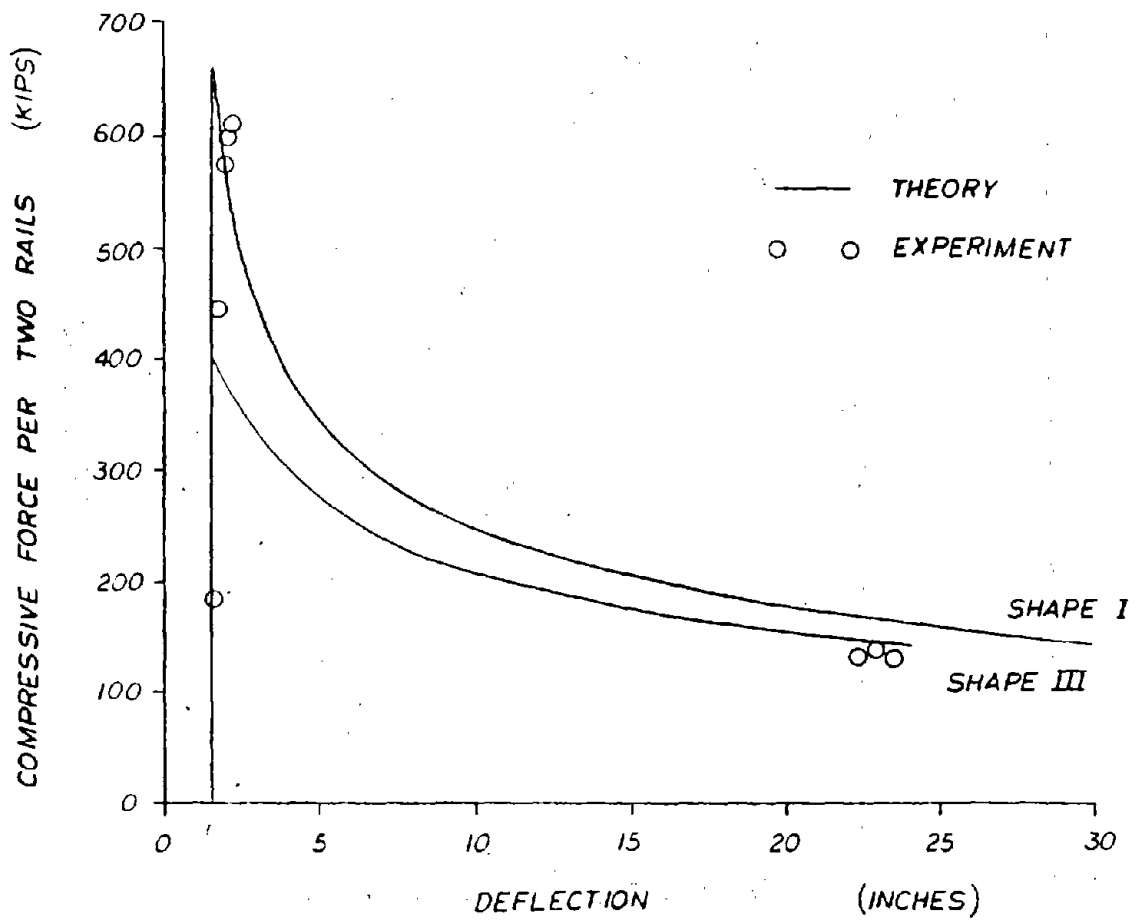


FIG. 17 - RAIL FORCE IN BUCKLED ZONE VERSUS MAXIMUM DEFLECTION (TANGENT TRACK)

It is interesting that the compressive force in the buckled zone is reduced by 80 percent after buckling. The force in the two rails before buckling was 616,000 lbs (280 metric tons); after buckling it fell to 132,000 lbs (60 metric tons), thus considerable strain energy in the track was released because of buckling.

6.3 BUCKLED WAVE SHAPE

Figure 18 shows the measured lateral deflections versus the theoretically predicted wave shapes. The experimental curve is not entirely symmetrical. The theoretical maximum deflection is slightly less than the test result. The theoretical and the observed wavelengths are in good agreement.

6.4 RAIL FORCE VARIATION

The longitudinal rail force buildup with temperature, as indicated by the strain gauges, has been plotted in Figure 19. The variation of the force along the track just before and just after buckling is also shown. In Figure 20, a comparison has been made between the theoretical and the test results. The agreement is satisfactory.

It must be noted that the compressive force levels before buckling, as recorded at SG₃ and SG₄ locations, follow the law $P = EA\alpha T$, showing that there was no longitudinal movement of the track at this place. From SG₄ to SG₉ (the end of the test section), the compressive force, before buckling, drops off almost linearly and is no longer determined by the simple relation $P = EA\alpha T$. This is in agreement with the general theory presented in Section 5, and is an important characteristic of finite tracks with finite end stiffness. It should be pointed out that in the case of the infinite track, constant force levels would exist before buckling, for uniformly heated rails.

The prebuckling forces in the central zone (as recorded by SG₂ and SG₁) are slightly less than that at SG₃. This can be

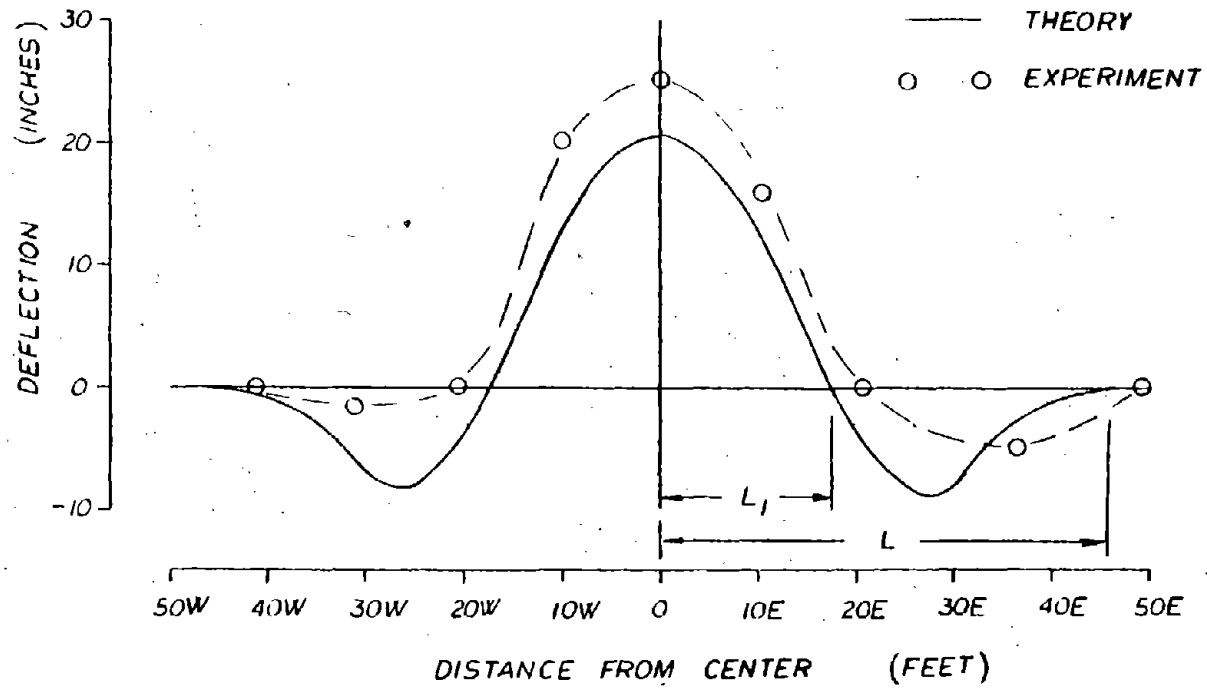


FIG. 18 - BUCKLED WAVE SHAPE III (TANGENT TRACK)

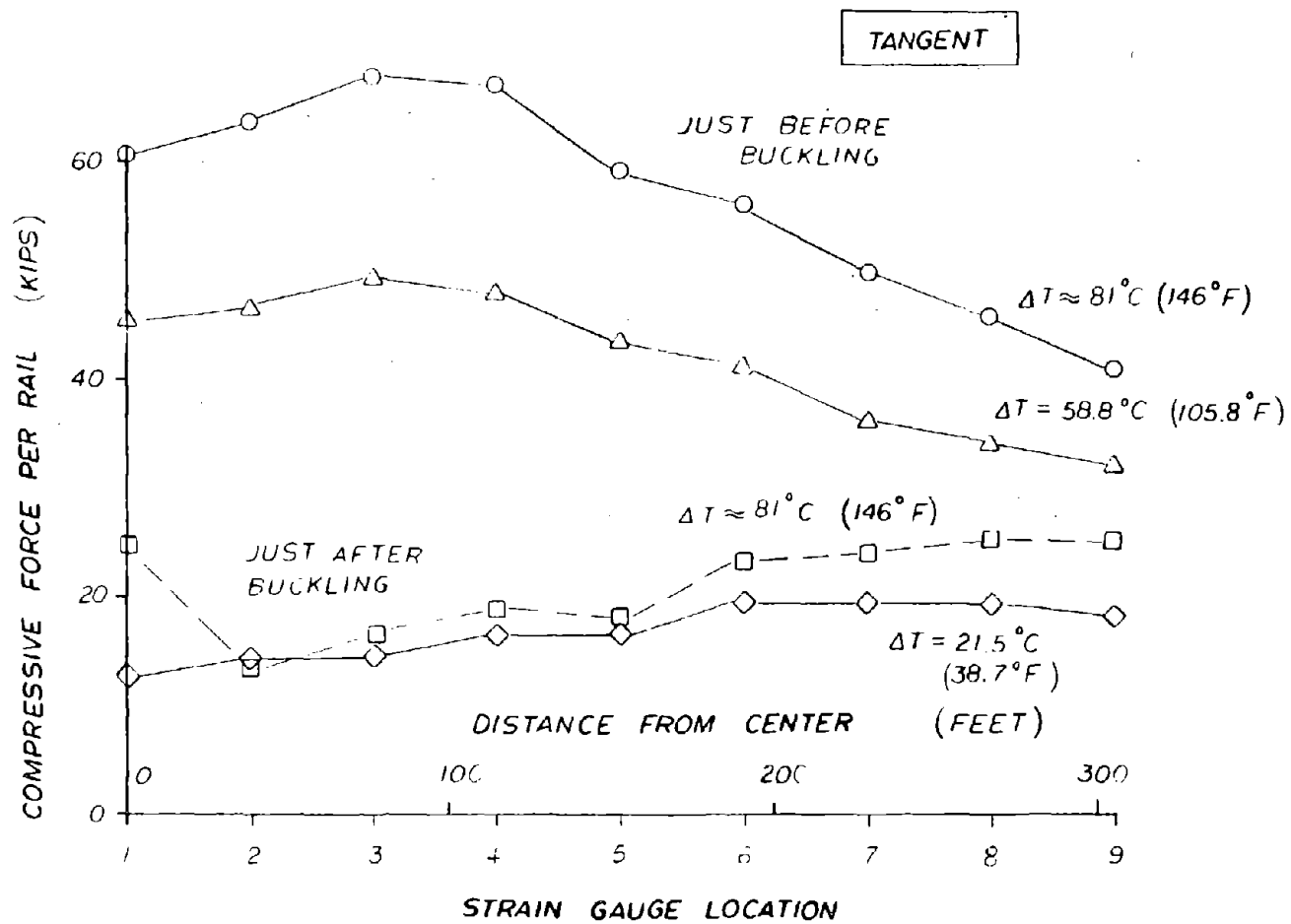


FIG. 19 - RAIL FORCE BUILDUP (TANGENT TRACK)

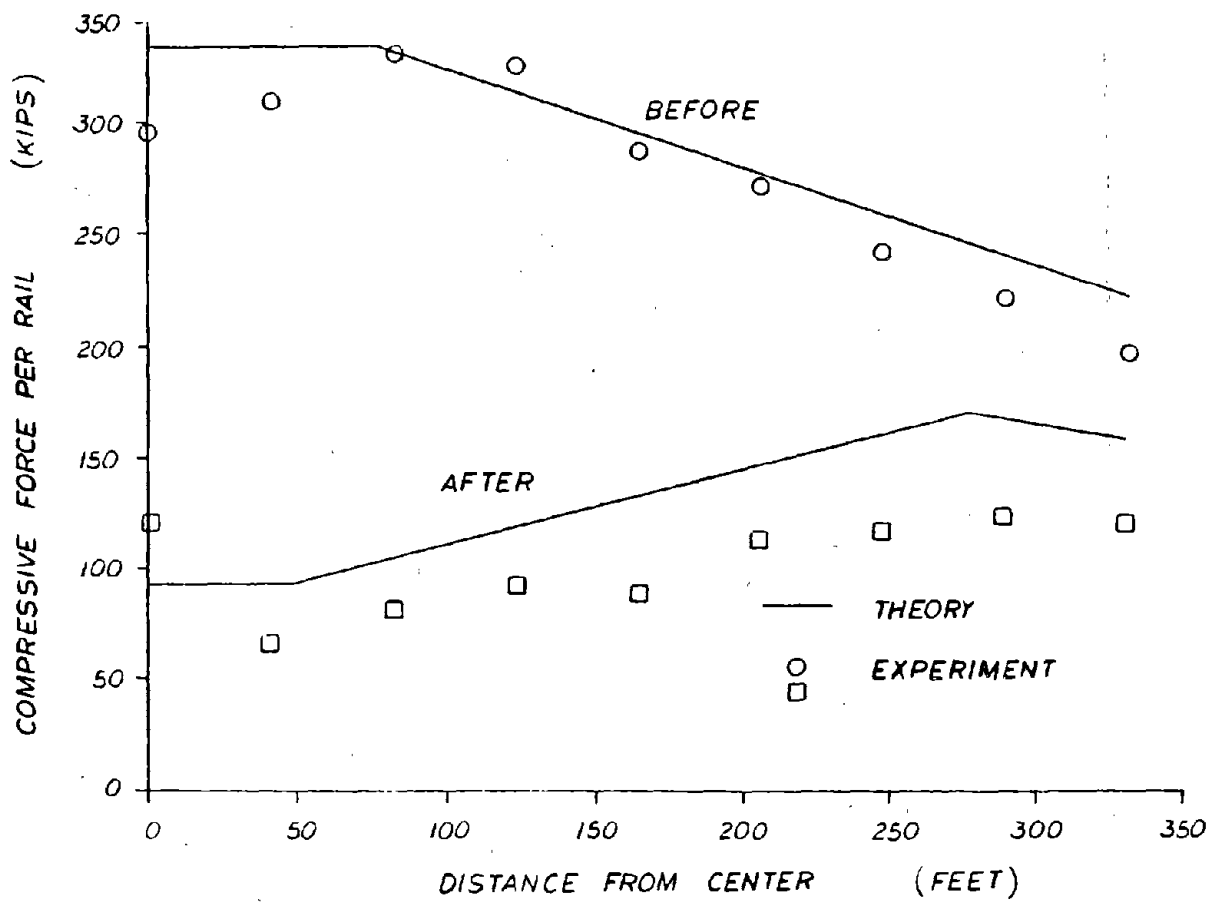


FIG. 20 - RAIL FORCE VARIATION BEFORE AND AFTER BUCKLING (TANGENT TRACK)

explained by the fact that the track relieves some of its compressive force due to the growth of imperfection with temperature increase.

As can be seen in Figure 19, the after-buckling reading SG_1 at the center showed a force level that is higher than SG_2 and SG_3 . It is believed that SG_1 reading became spurious after buckling because the rail yielded plastically at the center. Calculations, not presented here, indicated that the combined bending and the direct stress indeed exceeded the yield stress on one side of each rail base. The strain gauge was, of course, fixed on the web. Its reading was nevertheless in error, as the neutral axis must have been shifted from the original position and unsymmetrical bending effects could not be compensated by the strain gauge set.

It is believed that the correct value of the force at the center after buckling can be obtained by extrapolating the readings of SG_2 and SG_3 .

6.5 LONGITUDINAL DISPLACEMENT VARIATION

In the test, only three longitudinal displacement transducers were used. Two were located on one side of the track (U_1 and U_3). U_1 was at the end and U_3 was at about 183.7 ft. (56 m) away from the center. The data from the transducers, taken before and after buckling, are plotted in Figure 21. The theoretical curves are also shown in the figure.

The limited test data agree with the theoretical predictions reasonably. The expected maximum is around 1.57 in. (40 mm) towards the center, occurring outside the buckling zone at about 65.6 ft. (20 m) from the center. Unfortunately, no transducer was located here and this value could not be verified by the test data.

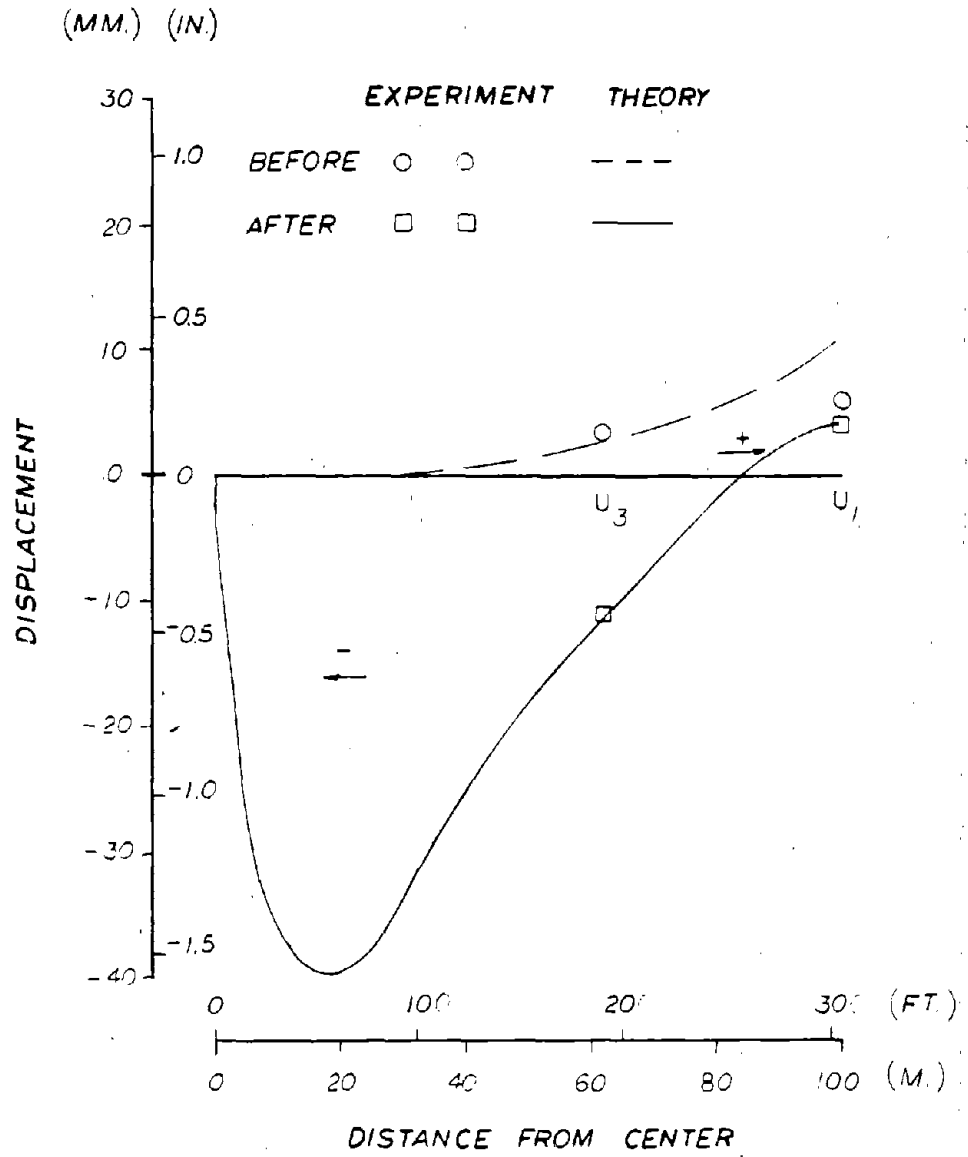


FIG. 21 - LONGITUDINAL DISPLACEMENT (TANGENT TRACK)

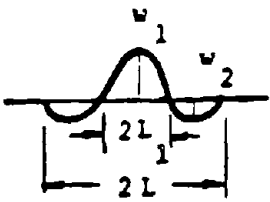
6.6 SUMMARY

1. A list of important results derived from the theory and the corresponding test values are presented in Table 5. It may be concluded that the overall agreement between the theory and the experiment is good.

2. The prebuckling compressive force distribution in a finite track with finite stiffness is different from that of the infinite track. In the latter, the force is constant along the track, whereas in the former, it drops off at the ends.

3. A symmetric imperfection produces a symmetric buckling mode. Based on other field tests, in general, Shape III seems to be the final mode for tangent track. Mode change from Shape I to Shape III can occur when the initial imperfection is of Shape I.

TABLE 5 - SUMMARY OF COMPARISON BETWEEN THEORETICAL AND EXPERIMENTAL VALUES (TANGENT TRACK)

ITEM		THEORY	EXPTL.
BUCKLING TEMPERATURE INCREASE ΔT_B ($^{\circ}F$)		135.9	146.2
PREBUCKLING FORCE* (KIPS)	CENTRAL ZONE	336.6	308.4
	ENDS	230.6	195.8
FORCE AFTER BUCKLING* (KIPS)	CENTRAL ZONE	76.6	66.9
	ENDS	149.6	123.4
BUCKLING LENGTHS AND DISPLACEMENTS	L (FT.)	47.6	49.5
	L_1 (FT.)	18.4	20.7
	W_1 (IN.)	20.5	22.4
	W_2 (IN.)	8.7	5.5
			
PREBUCKLING LONG. END DISPLACEMENT	U_1 (IN.)	+0.43	+0.24
POSTBUCKLING LONG. END DISPLACEMENT	U_1 (IN.)	+0.16	+0.16
PREBUCKLING LONG. DISPLACEMENT **	U_3 (IN.)	+0.12	+0.16
POSTBUCKLING LONG. DISPLACEMENT **	U_3 (IN.)	-0.47	-0.43

*FORCE PER RAIL

** 143.5 FT FROM U_1

7. CURVED TRACK ANALYSES

The curved test track results have also been compared to the theoretical predictions with the parameters as given in Table 2. Only mode Shape I will be considered in the theory, as there was no change of mode during buckling as was found in the tangent test.

7.1 TEMPERATURE-DEFLECTION RESPONSE

The theoretical and test results are presented in Figure 22, showing the theoretical buckling temperature increase to be 119°F (66°C) and the test value 115°F (63°C), indicating good agreement. The theoretical safe temperature increase is 86°F and is higher than the value for the tangent track due to the higher lateral and longitudinal resistance values in the curved track.

The theoretical deflection amplitude at the buckling temperature is 19.3 inches, whereas the experimental value was only 14.3 inches, hence the agreement in the post buckling portion of the response curve is not as good for the curved track, as it is for the tangent track.

7.2 RAIL FORCE-DEFLECTION RESPONSE

The compressive force in the rail as obtained from theory is shown plotted against the maximum central deflection in Figure 23 along with the actual test results. The theoretical buckling force is about 114 kips (250 metric tons) per two rails and the test value is 100 kips (220 tons). The experimental values follow the trends predicted by the theory. After buckling, the force level dropped to about 59 kips (130 tons), a 41% reduction from the prebuckling level.

7.3 BUCKLED WAVE SHAPE

The measured buckled wave shape is compared with the computed theoretical shape in Figure 24. The theoretical and test buckling lengths are in reasonable agreement, while the theoretical

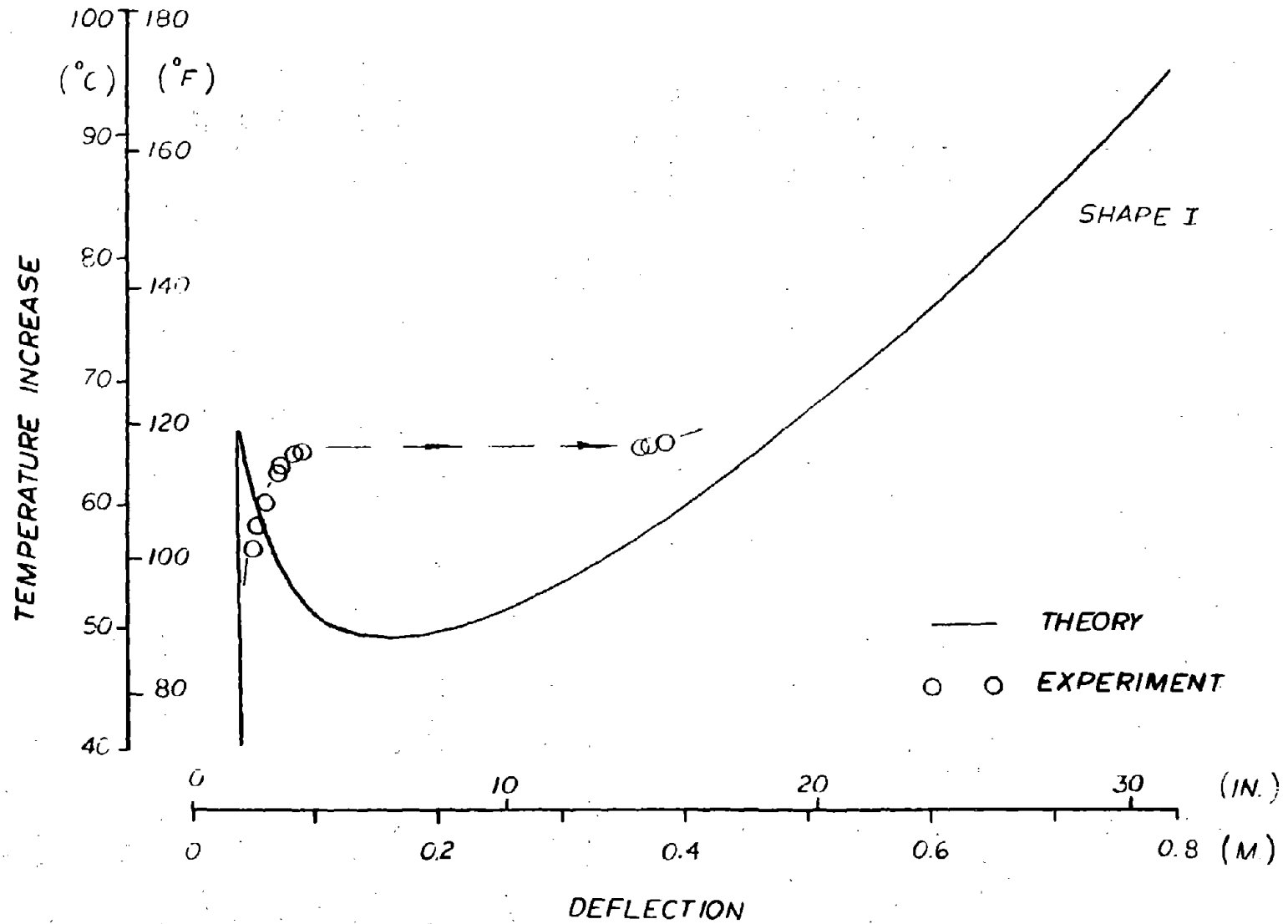


FIG. 22 - TEMPERATURE-DEFLECTION RESPONSE (CURVED TRACK)

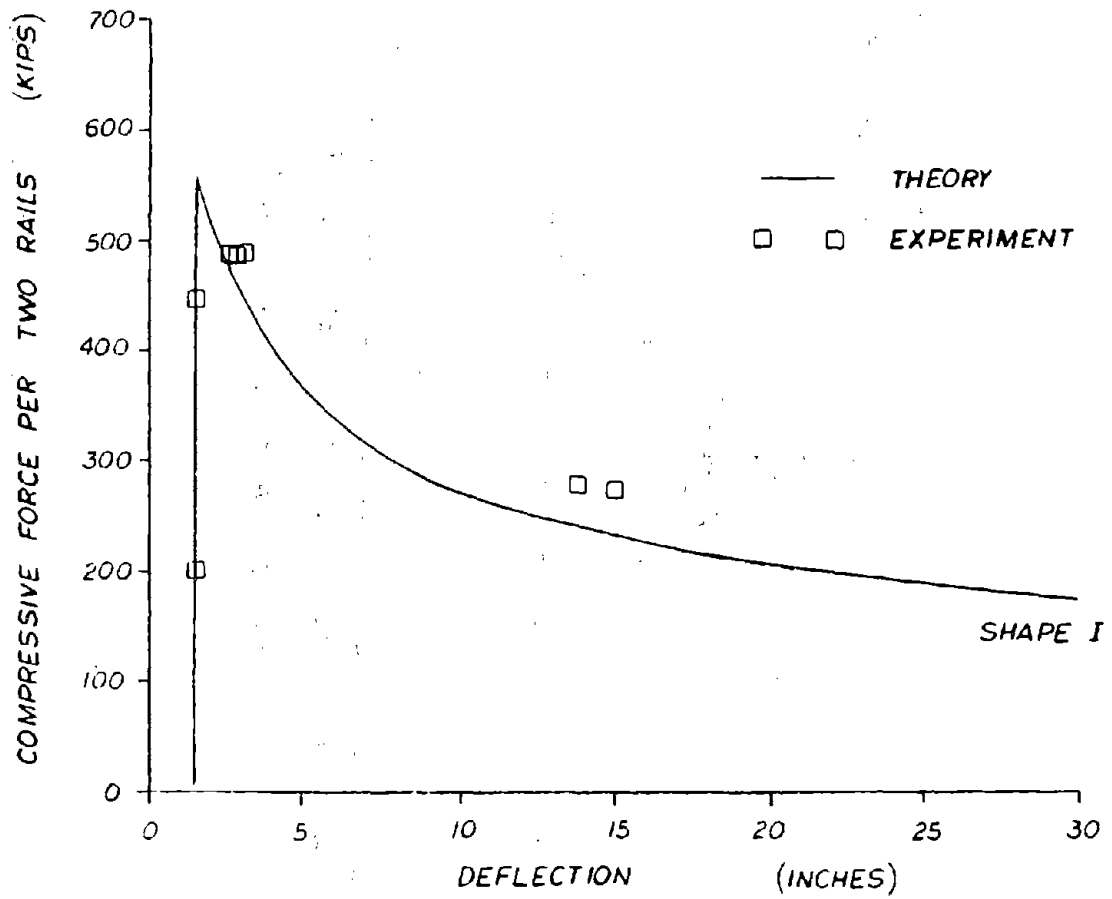


FIG. 23 - RAIL FORCE IN BUCKLED ZONE VERSUS MAXIMUM DEFLECTION (CURVED TRACK)

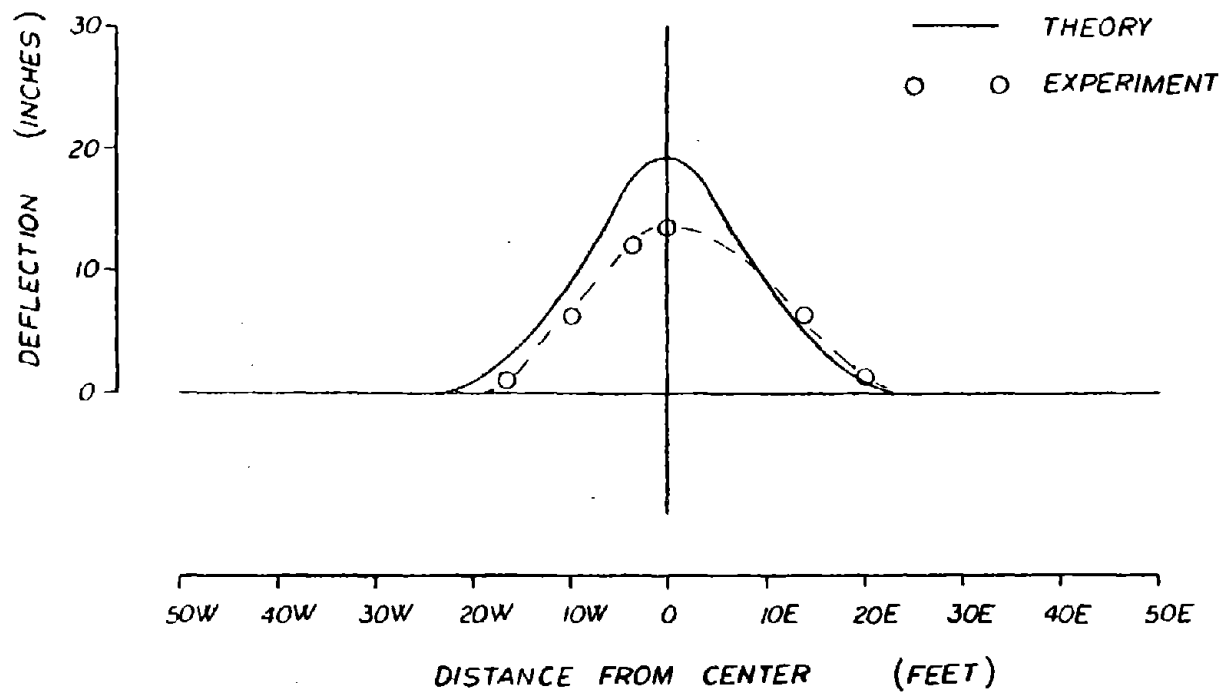


FIG. 24 - BUCKLED WAVE SHAPE I (CURVED TRACK)

buckling deflections are higher than the experimental deflections for the complete buckled zone. The agreement is not as good as for the tangent track.

7.4 RAIL FORCE VARIATION

The force built up in the rail with increase in temperature, as recorded by the strain gauges, is shown in Figure 25. In Figure 26, a comparison between the theory and the experiment for the forces just before and just after buckling is presented.

The force buildup at SG_4 location is almost according to the formula $P = AE\alpha T$, up to the instant of buckling. Hence, there are no tangential (longitudinal) movements of the track at this point. From SG_4 to SG_9 , the force drops off because of the end movement as expected in the theory. The force level indicated by SG_1 before buckling is smaller than SG_4 , since the former was situated in the imperfection zone, which grew and relieved the force slightly with increase in temperature. The force drop from SG_4 to SG_9 (end of the test section) is an important feature of the finite track with a finite stiffness.

The plastic yielding of the rails at the center, as in the tangent track, resulted in spurious readings of the central strain gauge SG_1 after buckling. Again, it is believed that the correct value of the force at the center can be obtained by the extrapolation of nearby strain gauge readings.

The overall agreement between the theory and the test regarding the rail force levels is satisfactory.

7.5 TANGENTIAL DISPLACEMENT VARIATION

The tangential (longitudinal) displacement of the track was monitored at three locations. Of these, two (U_1 and U_3) were on one side of the track.

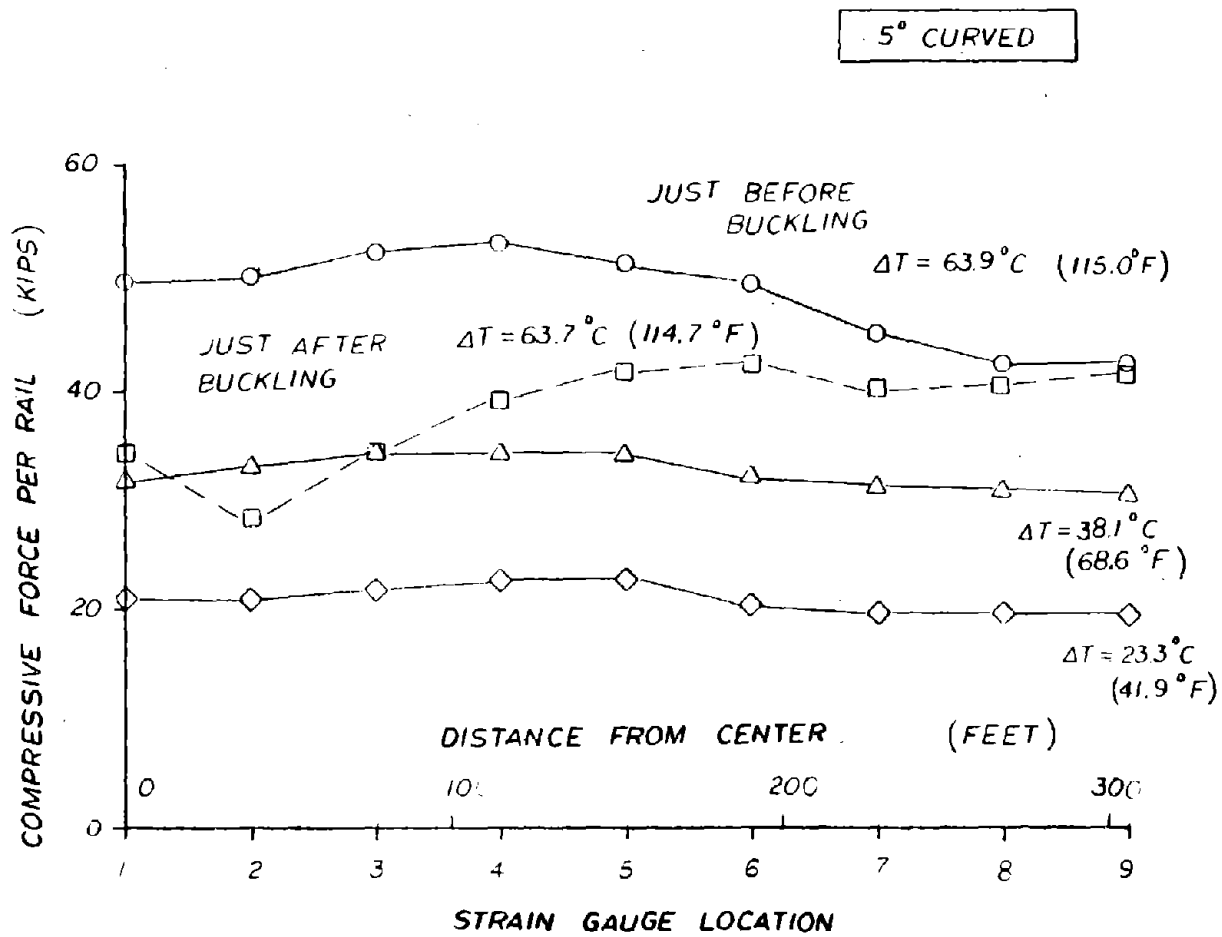


FIG. 25 - RAIL FORCE BUILDUP (CURVED TRACK)

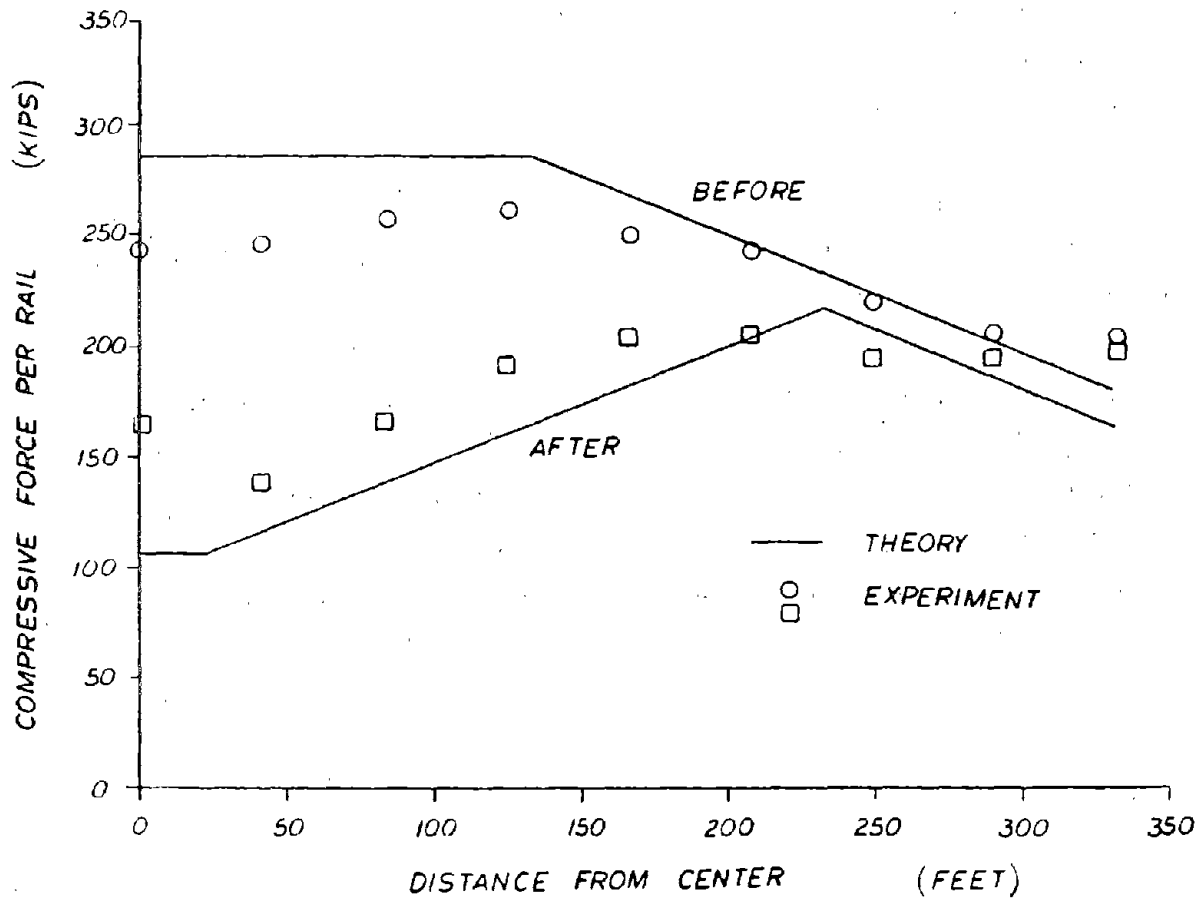


FIG. 26 - RAIL FORCE VARIATION BEFORE AND AFTER BUCKLING (CURVED TRACK)

The theoretical pre-and post-buckling distributions of the displacement are shown in Figure 27. The results of U_1 and U_3 are in reasonable agreement with the theory. The maximum theoretical post buckling displacement is about 0.91 in. (23 mm) towards the center of the buckle, occurring near the ends of the buckled zone.

7.6 SUMMARY

1. A summary of the important results from the theory and the experiment is presented in Table 6. The overall agreement between the theory and experiment is good.

2. A symmetric imperfection resulted into the Shape I symmetric buckling mode. Unlike the tangent track, the curved track did not change its mode during buckling.

3. The test track was instrumented for monitoring prebuckling radial (lateral) movement of the curved track. No significant movement was found. However, breathing of curves (radially inwards and outwards) with temperature fluctuations is reported to be a common phenomenon in certain practical tracks.

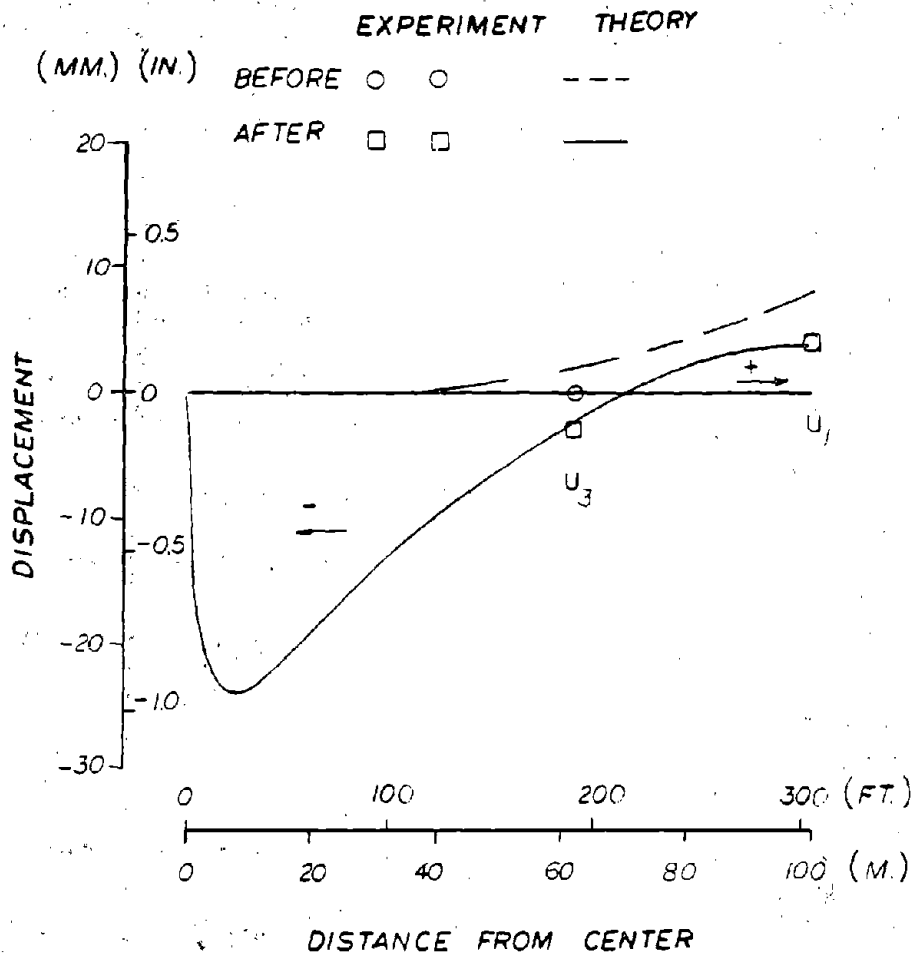
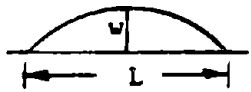


FIG. 27 - LONGITUDINAL DISPLACEMENT (CURVED TRACK)

TABLE 6 - SUMMARY OF COMPARISON BETWEEN THEORETICAL AND EXPERIMENTAL VALUES (CURVED TRACK)

ITEM		THEORY	EXPTL.
BUCKLING TEMPERATURE INCREASE ΔT_B ($^{\circ}F$)		119.3	115.4
PREBUCKLING FORCE* (KIPS)	CENTRAL ZONE	262.2	240.2
	ENDS	192.1	202.0
FORCE AFTER BUCKLING* (KIPS)	CENTRAL ZONE	103.4	136.8
	ENDS	159.5	197.3
BUCKLING LENGTHS AND DISPLACEMENTS 	L (FT.)	23.9	37.7
	W (IN.)	19.3	14.3
PREBUCKLING LONG. END DISPLACEMENT	U_1 (IN.)	+0.31	+0.20
POSTBUCKLING LONG. END DISPLACEMENT	U_1 (IN.)	+0.20	+0.20
PREBUCKLING LONG. DISPLACEMENT **	U_3 (IN.)	+0.04	0
POSTBUCKLING LONG. DISPLACEMENT **	U_3 (IN.)	-0.12	-0.12

*FORCE PER RAIL

** 143.5 FT FROM U_1

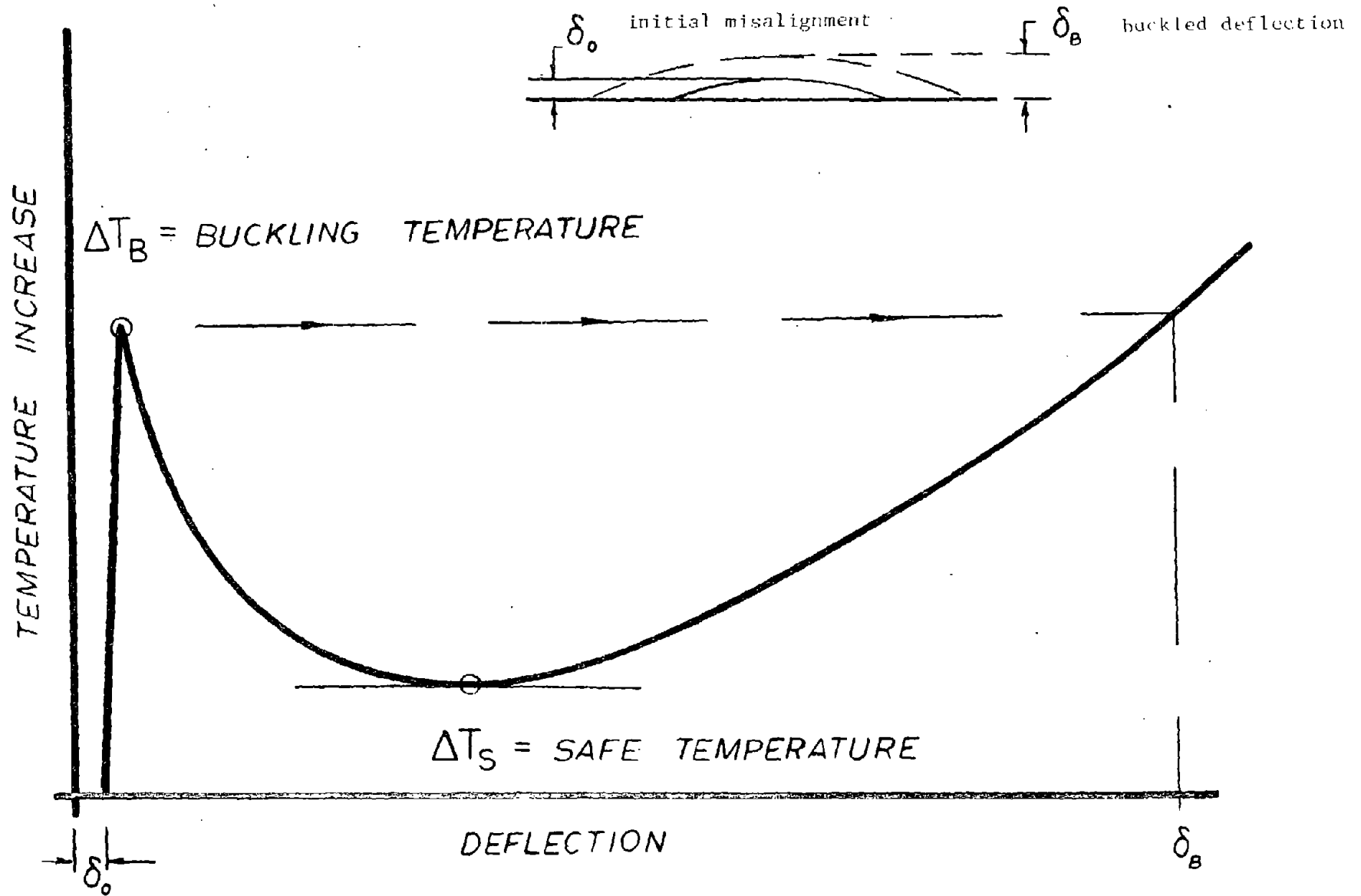


FIG. 28 - BUCKLED RESPONSE IN THE LATERAL PLANE (See Ref., p. 3)

8. CONCLUSIONS

(1) The current theory for analysis of thermal buckling is adequate for explaining the mechanism of track buckling under static conditions. The theory is in a highly developed state and should be useful to track maintenance and design engineers. It is now possible to study the effect of track imperfections, curvature, "finite" track (end restraints), missing ties, and other relevant parameters.

(2) Successful buckling test concepts and methodology have been established. The "mobile heating" technique developed can be used to facilitate rail heating tests on tracks in service. Measurement and recording data on rail compressive force, temperatures, and displacement can be carried out automatically. The importance of adequate test section length was manifested by the non-uniform force build-up and test section end displacements, resulting in the improvement of analytic predictions by including pre-buckled displacements and end-restraint parameters.

(3) Both tangent and curved tracks tested on the Southern exhibited relatively high buckling temperatures (above neutral), in spite of initial imperfections. The curved track exhibited a lower buckling temperature than the tangent, a less "explosive" type of buckling, and a smaller wave shape and amplitude.

(4) To properly simulate infinite track situations, especially with regard to the rail longitudinal force distribution, the heated length in the buckling tests will have to be greater than 656 ft. (200 m). At low temperature, the force distribution will be practically constant. As the temperature increases, the ends move out and the end effects influence larger portions of the test track. The force tapers off at the ends, the distribution eventually becomes trapezoidal at sufficiently high temperatures.

9. RECOMMENDATIONS

(1) The track lateral resistance, being the most important parameter, should be determined as accurately as possible. A simple and practical measurement technique is needed. Existing techniques such as single tie and panel tests are not suitable for service tracks. An approach based on the equilibrium equation has been presented here. Further investigations are required to establish the reliability of the technique.

(2) The present lateral pull rig is bulky and needs to be improved for easier handling and operation. The use of a bulldozer, from which the present rig derives its reaction, may not always be convenient and satisfactory as slipping may occur. Improvements are also needed in the rig for use in curved tracks with superelevation.

(3) Dynamic buckling tests on tracks with moving vehicles are required. The buckling and the safe temperatures under moving loads are suspected to be lower than the respective "static values." The effect of "precession" waves in liftoff and consequent reduction in the lateral resistance should be studied, as well as the influence of lateral loads.

(4) For given track parameters, a design criterion for assurance of safety against buckling is needed. One approach can be based on buckling temperature ΔT_B and a required factor of safety. Another approach can be based on the safe temperature ΔT_S . The first approach requires a knowledge of maximum expected track imperfections. The second tends to be somewhat conservative.

Design data should be prepared in the form of charts and graphs giving both the buckling and the safe temperatures for a range of track parameters.

(5) Only two fully instrumented static tests have been conducted in the U.S., whereas, the total number of buckling tests conducted abroad seems to be in excess of 1000. The major portion of the work done on this subject in the U.S. has been devoted to the research methodology rather than to data generation. Since considerable advances have been already made in the theory, data generation can be made with the help of the theory, and only a limited number of additional tests (static and dynamic) need to be done to resolve the issues brought out in this report.

REFERENCES

1. "Accident/Incident Bulletin #149, Calendar Year 1980," June 1981, FRA/DOT Report.
2. A.M. Zarembski and G.M. Magee, "An Investigation of Railroad Maintenance Practices to Prevent Track Buckling," AAR Report #R-454, November 1980.
3. American Railway Engineering Association - Bulletin 670, p. 179, November-December 1978, Manual Recommendations.
4. A.D. Kerr, "Lateral Buckling of Railroad Tracks Due to Constrained Thermal Expansions - A Critical Survey," Proceedings of a Symposium on "Railroad Track Mechanics and Technology," Pergamon Press, 1978.
5. A.D. Kerr, "Analysis of Thermal Track Buckling in the Lateral Plane," FRA Report OR&D-76-285, 1978.
6. G. Samavedam, "Buckling and Post Buckling Analyses of CWR in the Lateral Plane," British Railways Board, R&D Division, Technical Note TN-TS-34, January 1979.
7. O. Ammann and C.V. Gruenewaldt, "Tests of the Effect of Axial Forces in Track," in German, Organ fur die Fortschritte des Eisenbahnwesens, Heft 6, 1933.
8. J. Nencsek, "Tests of the Royal Hungarian National Railroads on Track Stability," in German, Organ fur die Fortschritte des Eisenbahnwesens, Heft 6, 1933.
9. F. Birmann and F. Rabb, "On the Development of Continuously Welded Track - Test Results of the Karlsruhe Test Facility; Their Analysis and Interpretation," in German, Eisenbahntechnische Rundschau, 1960.

10. D.L. Bartlett, "The Stability of Long Welded Rails," Parts I-IV, Civil Engineering and Public Works Review, 1970.
11. E. Nemesdy, "Analysis of Horizontal Track Buckling in Accordance with the New Hungarian Tests," in German, Eisenbahntechnische Rundschau, Heft 12, 1960.
12. J. Nagy, "Experimental Investigations on CWR Track Behavior Due to Thermally Induced Loads, V and VI," in Hungarian, 1970 and 1974 Yearbook of the Railway Scientific Institute.
13. E.M. Bromberg, "The Stability of Jointless Track," in Russian, Izd Transport, Moscow, 1966.
14. G. Samavedam, "Analyses of Buckling Experiments at Old Dalby - Part I," Technical Memorandum, TMTS 114, R&D Division, British Railways Board, August 1980.
15. A.D. Kerr, "On Thermal Buckling of Straight Railroad Tracks and the Effect of Track Length on the Track Response," Rail International, September 1979.
16. G. Samavedam, A. Kish, and D. Jeong, "Parametric Studies of Lateral Stability of CWR," in preparation.
17. A. Kish, "Test Requirement Definition for Track Buckling Tests," DOT/TSC, January 1981.
18. Test Plan for Track Buckling Experiment, prepared by Foster-Miller Associates, Inc., DOT-7851, April 1981.

APPENDIX A
ADDITIONAL BUCKLING TESTS AT THE PLAINS, VA

The Southern Railway (SR) desired additional information on the buckling strength of curved tracks. Four additional tests were conducted without instrumentation on the same or adjacent track used in the two major tests described in this report. A summary of the results obtained in the four tests is presented in Table 7.

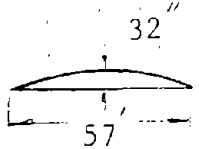
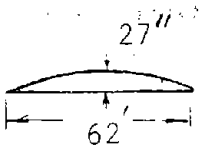
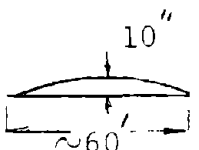
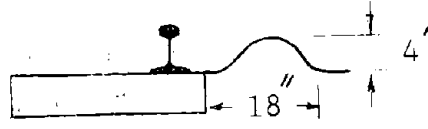
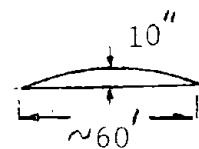
In comparison with the curved track tests previously described in this report which had a buckling temperature of approximately 110°F, the SR test #1 had a much higher buckling temperature (estimated at 200°F). This difference may be explained by the facts that the test track for the SR test #1:

- (1) had no visible imperfection
- (2) had a higher longitudinal resistance due to every tie being box anchored
- (3) was in the "as is" consolidated condition and was, therefore, probably at a higher lateral resistance
- (4) was shorter [i.e., 492 ft. (150 m) vs. 656 ft. (200 m)]

SR test #2 yielded lower buckling temperature (estimated at 136°F) than SR test #1 for the following possible reasons:

- (1) The test track was basically in a newly maintained condition following restoration after the TSC test, thus, having weakened resistance.
- (2) The rails yielded plastically in the TSC test, and although the track was re-aligned, a residual imperfection ("memory") would have been built up in the rail

TABLE 7 - SUMMARY OF SR BUCKLING TESTS*
(CURVED TRACK)

TEST NO.	TRACK CONDITION	T_B ABSOLUTE	ΔT_B ESTIMATED	BUCKLED SHAPE
1	14-16 IN. BALLAST SHOULDER; HEATED ZONE APPROX. 150 M.; EVERY TIE BOX ANCHORED	240°F	200°F	
2	REALIGNED, SURFACED, TAMPED, AFTER TSC TEST; EVERY TIE BOX ANCHORED; NO NOTICEABLE END MOTION	208°F	136°F	
3	REALIGNED AFTER PREVIOUS SR TEST #2; BALLAST REMOVED FROM HIGH RAIL TIE ENDS; RESULTED IN <u>PROGRESSIVE</u> BUCKLE.	185°F ↓ 100°F	113°F ↓ 78°F	
4	SAME TEST LOCATION AS SR TEST #3; BUCKLED ZONE REALIGNED TO ABOUT 7°; BALLAST SHOULDER BUILT UP;  EXPLOSIVE BUCKLE; MODE SHAPE AMPLITUDE 10"	174°F	102°F	

*TRACK PARAMETERS NOT MEASURED. NO DELIBERATE ATTEMPT MADE TO INCORPORATE IMPERFECTION. RADIUS OF CURVATURE = 350 M.

and ballast. This would result in a lower buckling temperature.

- (3) The SR test #2 was performed on a longer test section than SR test #1 [i.e., 656 ft. (200 m) vs. 492 ft. (150 m)].

SR test #3 resulted in a progressive buckle (i.e., ΔT_B did not exist) as one would expect because of the combined actions of:

- (1) built-in residual imperfection resulting from plastic yielding in the TSC test and the SR test #2, and
- (2) reduced lateral resistance (shoulder was removed).

SR test #4 resulted in an explosive buckle. By reinstating the shoulder (18") with additional shoulder height above the tie surface the lateral resistance was increased and ΔT_B becomes greater than ΔT_S . Other than the nature of the buckle (i.e., progressive versus explosive of SR test #3 versus SR test #4), no other conclusion can be drawn.

APPENDIX B
PILOT TESTS AT CHATTANOOGA

In 1979, two pilot tests on track buckling were carried out on a section of the Southern Railway's Yard in Chattanooga, TN. Apparently, these were the first tests on track buckling in the U.S. railroad history.

The main objectives of the test were:

- (1) to demonstrate the feasibility of causing track buckling by direct electric resistance heating of rails, the current being derived from diesel-electric locomotives.
- (2) to obtain a qualitative understanding of the buckling mechanism, in particular, its sensitivity to track imperfections.
- (3) to assess instrumentation requirements for future tests for quantitative studies.

Prior to the tests, two GP38-2 locomotives were modified; the same modification procedure was followed in the later tests at The Plains, VA, as described in the document [18]. The locomotives were stationed at one end of the test section, and a locomotive and hopper cars at the other end, with the hope of providing some restraints against possible longitudinal movements at the end of the test section.

Test Site Description and Preparation

The test section selected was a 328-ft.-long (100 m) CWR wood tie track located in the Southern Railway Systems' Butts Yard in Chattanooga. The test section contained 165 ties, slag ballast with an approximate shoulder width of 8 in. on the weaker (west rail) side, and 112 lb AREA rail. This section ran north-

south, bordered by a bridge on the north and a crossing at the south end.

A week prior to testing, the rails in the test section were cut and de-stressed at 59°F, anchors were re-applied at every other tie and four insulated joints were installed at the ends. The test section could be described as nearly perfectly straight with a barely discernible "bulge" toward the west, with three minor local misalignments (one at each end and one in the middle).

Test Section Instrumentation and Deployment

Instrumentation consisted of five lateral displacement transducers deployed in the central portion of test section approximately 20 feet apart, four longitudinal displacement transducers (one on each rail at both ends), and 10 resistance temperature transducers (five on each rail) approximately 80 feet apart. All data were continuously recorded on strip chart and analog tape. Center displacement and temperature were monitored and tabulated via digital voltmeter. In addition, stakes driven into the ground and connected by taut string were utilized to record pre- and post-buckling shapes. Other measurements included monitoring vertical liftoff, relative longitudinal rail to tie motions, and rail frequency response to axial load.

First Test (nominally straight track)

The first test run commenced at 10:20 a.m. on December 18, 1979, at an ambient temperature of 32°F and at a rail temperature of about 40°F. Prior to test initiation, the loose spikes (on approximately 50 ties) were driven in. In the center zone where some rail uplift was observed, the ties were slightly lifted and spiked down.

Nothing noticeable was observed up to about a rail temperature of 150°F. At about 180°F, the end regions (about 60 feet from each end) exhibited about 1/8" to 1/4" relative longitudinal

rail to tie displacement, the ends being about 1/4 in. At 260°F, relative rail to tie displacements increased to about 1/2 in. At 303°F with a sudden violent bang, a sudden longitudinal shift toward the north occurred in the central region with a simultaneous buckle at the north end of the test zone. The buckled shape was of the Shape III type. The total heating time was approximately one hour.

The buckle occurred directly in front of the end restraint locomotive; the insulated joints suffered some rotation and rails under the locomotive a slight misalignment. Approximate length of the buckle was 70 feet and approximate amplitudes of the first and second waves were 27 inches and 20 inches respectively. A longitudinal shift of about 1 inch and 2 inches at 130 ft. and 100 ft. from the joint, respectively, could be observed after the buckle. The estimated axial force induced in the rails prior to buckling was about 262 tons per rail. The location of the anticipated buckle was not known a priori; its occurrence near the end restraint locomotive suggests that the laterally weakest portion of the track was in that zone. It is possible that the installed joints, coupled with some vertical uplift induced by the end restraint dead weight, and the presence of a slight lateral misalignment caused this local weakening.

Second Test (imperfect track)

The buckled section in test #1 was "repaired" by pushing the track back into the straight shape. In order to prevent buckling from re-occurring in this weakened zone during the second test, two 39' rail segments were spiked adjacent to existing rails to provide additional strength. Additionally, two backhoe vehicles were positioned against the rails during the second test to provide added lateral restraint.

To induce the buckle in a prescribed location during the second test, a track lateral misalignment of 2-1/2' in. over a length of 56 ft. was induced. The second test commenced at 3:00 p.m.;

the rails had already cooled down to 69°F. At the rail temperature of 172°F (heating time of about 25 minutes), the track buckled out at the 2-1/2" misalignment in an asymmetrical mode shape III with a maximum amplitude of 14".

Conclusions

The following conclusions are drawn from the two tests.

(1) Two locomotives are capable of developing the power required (7,000 amperes at about 50 volts) for track buckling; an average heating rate of about 5°F/min. was maintained through the test.

(2) A nearly "perfect" track (very slight lateral imperfections) required a very high temperature change to induce buckling (of the order of 245°F).

(3) The influence of an artificially induced 2.5 inches of lateral misalignment over a chord length of 56 feet resulted in a more than 50 percent reduction in the buckling temperature as compared to the "perfect" track.

(4) The locomotives and the hopper car could not provide enough restraint against longitudinal movements of the rail at the ends. The test length, 328 ft. (100 m), might not be sufficient.

APPENDIX C

PHOTOGRAPHS OF THE PLAINS, VA, TRACK BUCKLING TESTS



PHOTO. 1 - CURVED TEST SITE

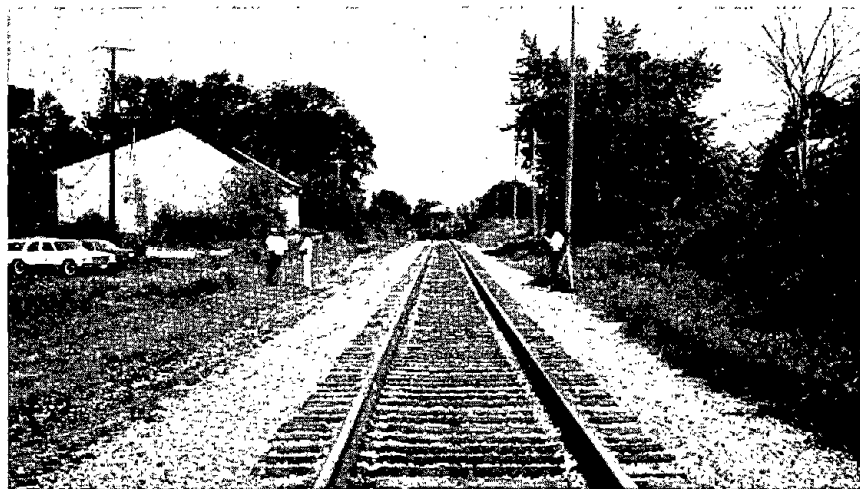


PHOTO. 2 - TANGENT TEST SITE

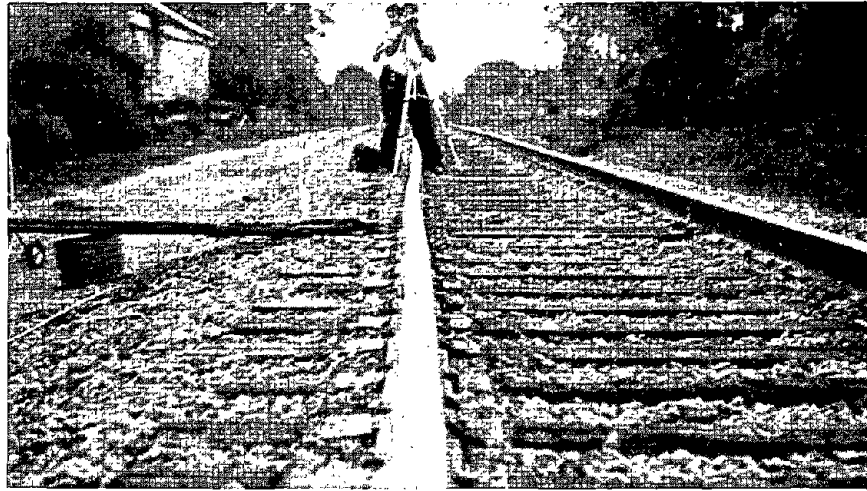


PHOTO. 3 - INITIAL MISALIGNMENT SETTING AND LATERAL RESISTANCE MEASUREMENT

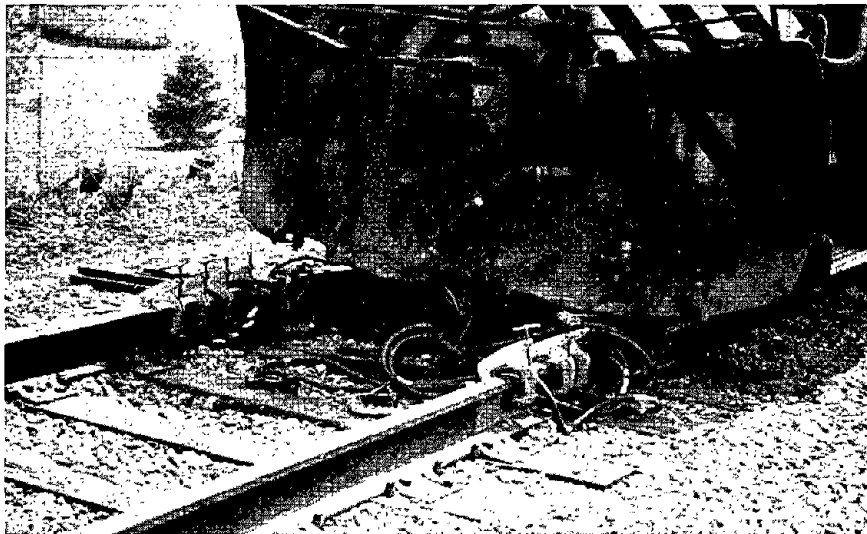


PHOTO. 4 - LOCOMOTIVE/ RAIL HEATING

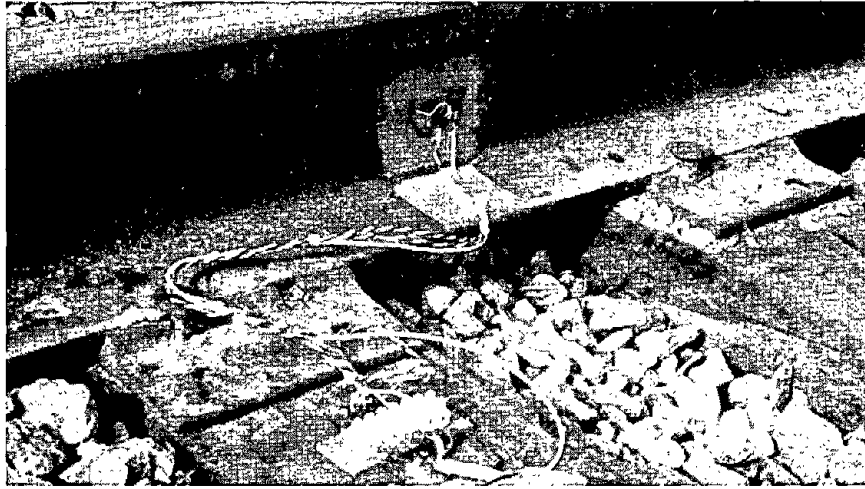


PHOTO. 5 - STRAIN GAUGE SET-UP



PHOTO. 6 - APPARATUS FOR SETTING INITIAL IMPERFECTION AND MEASUREMENT OF LATERAL RESISTANCE

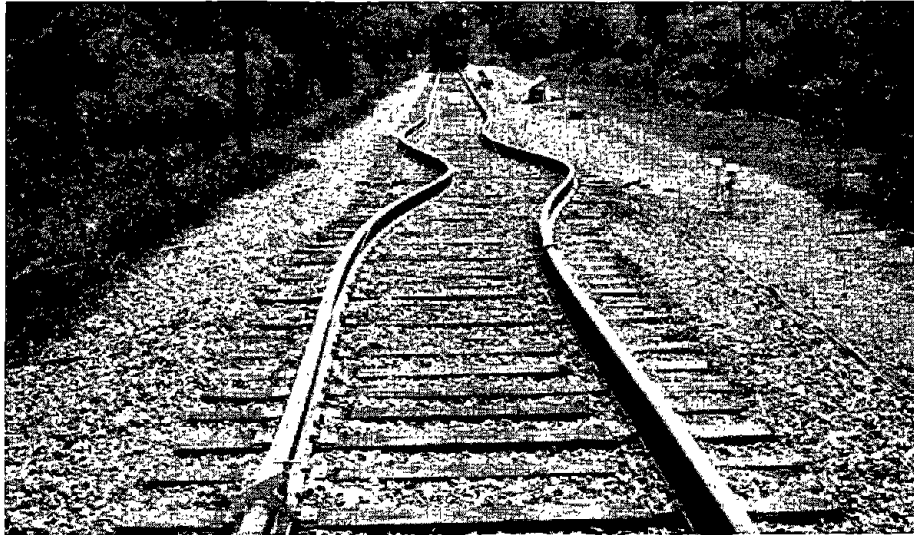


PHOTO. 7 - BUCKLED WAVE SHAPE III (TANGENT TRACK)

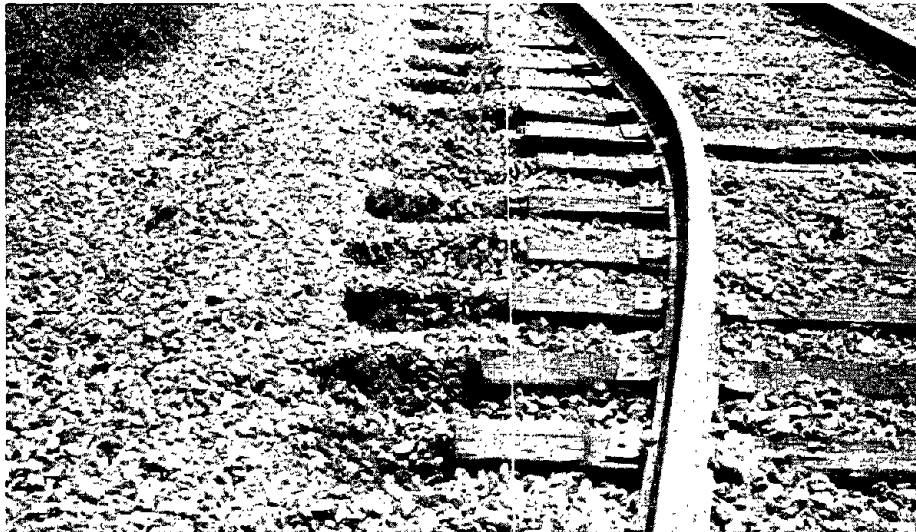


PHOTO. 8 - BALLAST DISTURBANCE FROM BUCKLED SHAPE
(TANGENT TRACK)

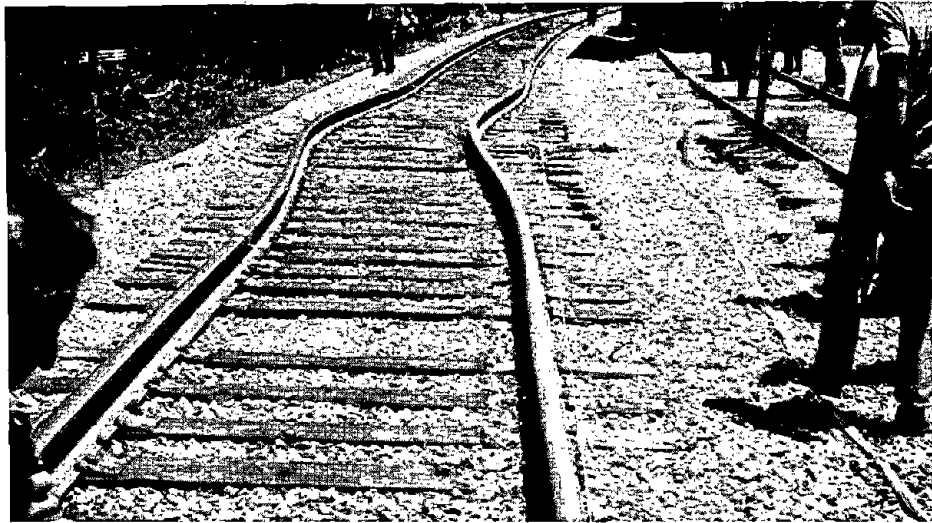


PHOTO. 9 - BUCKLED WAVE SHAPE I (CURVED TRACK)

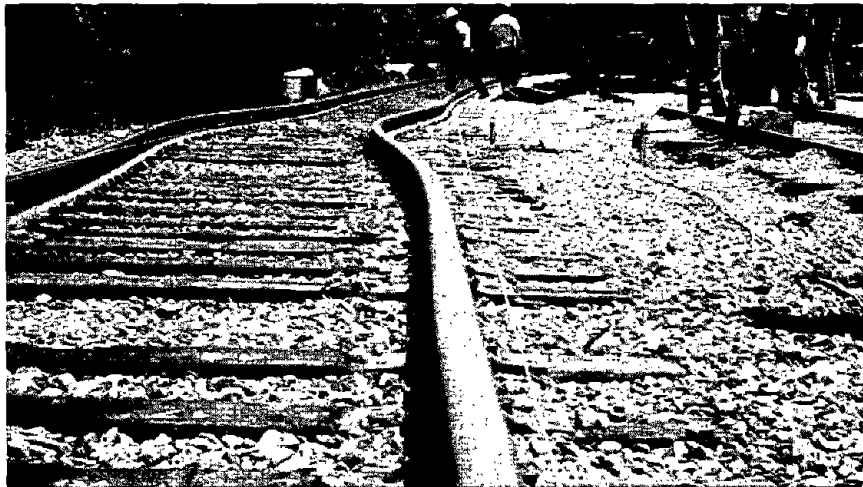


PHOTO. 10- BUCKLED WAVE SHAPE FROM CURVED TEST